Online Convex Optimization of Multi-energy Building-to-grid Ancillary Services

Antoine Lesage-Landry, *Member, IEEE,* Han Wang, *Student Member, IEEE,* Iman Shames, *Member, IEEE,* Pierluigi Mancarella, *Senior Member, IEEE,* and Joshua A. Taylor, *Member, IEEE*

***Abstract*—In this work, buildings with several sources of flexibility, subject to multiple energy requirements, and having access to different electricity markets are considered. A two-level algorithm for optimizing the building's energy management under uncertainty and limited information is presented in this paper. A mixed-integer linear program scheduling level is first used to set an energy management objective for every hour using only averaged data. Then, an online convex optimization algorithm is used to track in real-time the objective set by the scheduling level. For this purpose, a novel penalty-based online convex optimization algorithm for time-varying constraints is developed. The regret of the algorithm is shown to be sublinearly bounded above. This ensures, at least on average, the feasibility of the decisions made by the algorithm. A case study in which the two-level approach is used on a building located in Melbourne, Australia is presented. The approach is shown to satisfy all constraints 97.32% of the time while attaining a positive net revenue at the end of the day by providing ancillary services to the power grid.**

***Index Terms*—multi-energy systems, flexibility, ancillary services, online convex optimization, time-varying constraints**

I. Introduction

MULTI-ENERGY systems (MESs) couple multiple energy sectors, e.g., electricity, heating, cooling, and transportation [1], [2]. Buildings are a significant class of MES, and can provide useful services to the power grid while increasing their own revenues [3], [4]. In this work, we focus on buildings as MESs. This is a challenging optimization problem due to its high dimensionality and its multiple sources of uncertainty.

We propose a real-time decision algorithm to optimize the energy consumption of a multi-energy system under uncertainty. Several sources of flexibility are available to the MES: the building's thermal inertia, battery energy storage, thermal energy storage of water. The MES is also subject to several uncertain and time-varying requirements: indoor temperature regulation, domestic hot water demand, and electric baseload demand. The MES can import and export electricity from and to the grid and generate power from its own photovoltaic (PV) panels.

By leveraging its flexibility, a multi-energy building can contribute to different ancillary services, e.g., contingency services, benefiting the network and generating additional revenue for the building. For example, building-to-grid flexibility could be used by the system operator for fast frequency response, regulation or power balancing services and thus improve the grid's stability and resiliency of renewable-powered grids [3], [5]. A building must have some communication and control capabilities to provide these services, e.g., measurements of indoor temperature and the ability to send instructions to its cooling system. In this paper we propose a real-time algorithm for one or multiple buildings to provide ancillary services.

We propose a two-level algorithm consisting of a level for lookahead planning under limited information using a mixed-integer linear program (MILP) and a real-time decision level based on online convex optimization (OCO). We design a novel OCO algorithm for time-varying feasible sets to decide the building's energy usage in real-time. This allows the MES to deal with time-varying and uncertain constraints like intermittent PV generation while optimizing its energy usage. The approach is flexible due to its real-time decision process and requires relatively little information: only the building's parameters and approximate information about its environment and users are needed. Our two-level algorithm is not computationally demanding and can be used to aggregate several buildings together to provide network-level ancillary services. We test our approach on a building located in Melbourne, Australia.

Related work. Several authors have designed static or offline computation-based approaches for providing flexibility with buildings [6]–[11]. Uncertainty was considered using stochastic optimization in [8] but not in real-time. In [12], the authors aggregated several MES at the community level and computed its financial value using an offline MILP without uncertainty. We use their aggregated MES model, but only assume access to the building's parameters and a rough estimate of unknowns like mean temperature and solar irradiance.

Model predictive control (MPC) [13], [14] is a related approach that has been used for real-time MES optimization under uncertainty [15]–[17]. In this context, MPC-based approaches require accurate information about the loads, consumer, environment and significant time for computation. This motivates our use of OCO [18], [19], which requires minimal information and computation time. OCO has been previously

This work was funded by the Fonds de recherche du Québec – Nature et technologies, the Ontario Ministry of Research, Innovation and Science and the Natural Sciences and Engineering Research Council of Canada.

A. Lesage-Landry is with the Energy & Resources Group, University of California, Berkeley, CA, USA (e-mail: alesagelandry@berkeley.edu).

J.A. Taylor are with The Edward S. Rogers Sr. Department of Electrical & Computer Engineering, University of Toronto, Toronto, Ontario, Canada, M5S 3G4. e-mail: josh.taylor@utoronto.ca.

H. Wang, I. Shames and P. Mancarella are with the Department of Electrical and Electronic Engineering, The University of Melbourne, Melbourne, Australia. e-mail: {wangh12@student., iman.shames@, pierluigi.mancarella@} unimelb.edu.au. This work was partly done while A. Lesage-Landry was visiting The University of Melbourne.

used for demand response in power systems [20], [21]. To the best of the authors' knowledge, OCO has not to date been used to optimize MES.

Our specific contributions are:

- We propose a two-level algorithm to manage an MES in real-time and under uncertainty (Section IV).
- We propose a new OCO algorithm for time-varying constraints and provide a sublinear regret bound for the algorithm (Section IV-C).
- We test our two-level algorithm in a case study based on a building in Melbourne, Australia (Section V) and compare its performance to a model predictive control-based approach (Section V-C).

We first detail the models used for different buildings' systems in Section II. The scheduling level of our approach is presented in Section III followed by the tracking level in Section IV. We present an analysis of the new OCO algorithm in Section IV-C. A detailed case study is presented in Section V and the performance of the two-level approach is shown. We conclude by highlighting the key points of our approach in Section VI.

II. MES MODELING

We present our two-level algorithm for managing building energy consumption under uncertainty. In this work, uncertainty takes the form of inexact information, e.g., about natural phenomena such as weather forecast, and is modeled using random variables.

The first level is a scheduling program. The goal of the scheduling program is to use predictions, e.g. electric market average data, to plan an energy consumption trajectory that maximizes the building benefits while satisfying its constraints. This is formulated as a mixed-integer linear program. The output of the scheduling MILP is a sequence of energy consumption objectives for the building to follow in the second level of the algorithm. The second level on the algorithm is an OCO-based real-time tracking algorithm. Each scheduling round is then split into tracking rounds of the order of less than a minute. The tracking algorithm manages the energy resources on a short time-scale to the follow objective set by the scheduling algorithm. Between tracking rounds, the algorithm observes the building parameters and adapts its next decision accordingly. This allows the tracking algorithm to deal with the different sources of uncertainty like weather, scheduling prediction error and unpredictable human behavior.

We define two separate timescales. Let $T = 1, 2, \dots \tau$ be the scheduling round index and τ be the scheduling horizon. The scheduling rounds represent time intervals H of an hour in our case study. Let $t = 1, 2, \dots F$ be the tracking round index, where F is the number of tracking round in each scheduling round. The tracking rounds represent time intervals h of thirty seconds. The scheduling and tracking timescales are summarized in Figure 1.

Let R be the number of energy flows into, out of, and utilized by the building and S be the number of services

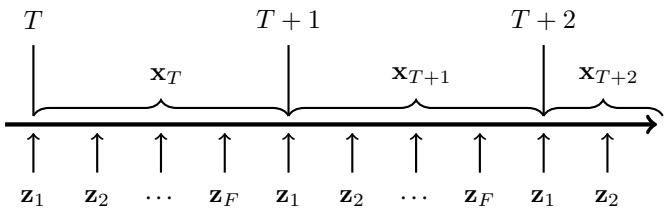

Fig. 1. Scheduling rounds & decisions (top) and tracking rounds & decisions (bottom)

the building can offer. Let $\mathbf{x}_T \in \mathbb{R}^R$ be the energy resource decision variable during scheduling round T such that

$$\mathbf{x}_T = \Big(x_{T,\text{import}} \;\; x_{T,\text{export}} \;\; \mathbf{s}_T^\top \;\; x_{T,\text{HVAC}} \;\; x_{T,\text{baseload}} \;\; x_{T,\text{EB}} \;\; x^{\text{c}}_{T,\text{BES}} \;\; x^{\text{d}}_{T,\text{BES}} \;\; x_{T,\text{TES}} \;\; p_T\Big)^\top,$$

where $\mathbf{s}_T \in \mathbb{R}^S$ and $\mathbf{s}_T = \big(s^+_{T,\text{reg}} \; s^-_{T,\text{reg}} \; s^+_{T,\text{fast}} \; s^-_{T,\text{fast}} \; s^+_{T,\text{slow}} \; s^-_{T,\text{slow}} \; s^+_{t,\text{delay}} \; s^-_{T,\text{delay}}\big)^\top$, the service vector. The components of $\mathbf{x}_T$ and $\mathbf{s}_T$ are detailed in Tables I and II.

The service vector represents the energy dispatched by the building to ancillary service. Frequency control ancillary services (FCAS) are used to maintain the system frequency within limits by maintaining the balance between demand and generation. More specifically, raise FCAS increases the frequency by increasing generation or reducing demand, while lower FCAS decreases frequency by decreasing the generation or rising demand.

In the Australian National Electricity Market (NEM), there are two types of FCAS: regulation FCAS and contingency FCAS. Regulation FCAS is used to continuously correct minor frequency deviations, while contingency FCAS is used for larger deviations [22]. The contingency FCAS is further grouped into fast (respond within 6 seconds and maintain the service for 60 seconds), slow (respond within 60 seconds and maintain the service for 5 minutes), delayed (respond within 5 minutes and maintain the service no longer than 10 minutes) contingency FCAS. The FCAS providers are paid for their availability, regardless of whether they are called.

The following four subsections present the scheduling round constraints, which are taken from [10]–[12]. Each can be converted to the corresponding tracking round constraint by substituting t for T and h for H.

A. Building requirements

The building requirements are as follows. The temperature θ_T at each scheduling round T must stay inside a pre-defined interval set by the building users:

$$\underline{\theta} \leq \theta_T \leq \overline{\theta}, \tag{1}$$

where $\overline{\theta}$ and $\underline{\theta}$ are the maximum and minimum temperatures. The maximum and minimum temperature constraints can be a function of the occupancy of the building. When the building's occupants are absent, a wider temperature interval can be used to increase the flexibility of the load. In this work, we set the temperature constraints to be constant throughout the day. The

TABLE I
BREAKDOWN OF $\mathbf{x}_t$

Component	Detail (kWh)
$x_{T,\text{import}}$	Energy purchased by the building
$x_{T,\text{export}}$	Energy sold by the building
$\mathbf{s}_T$	Ancillary services provided by the building
$x_{T,\text{HVAC}}$	Energy used to regulate the building temperature by the heat, ventilation and air conditioning (HVAC) system
$x_{T,\text{baseload}}$	Energy used to satisfy the building electric baseload demand
$x_{T,\text{EB}}$	Energy dispatched to the electric water boiler (EB)
$x^{\text{d}}_{T,\text{BES}}$	Energy taken out of the battery energy storage (BES)
$x^{\text{c}}_{T,\text{BES}}$	Energy use to charge the battery energy storage
$x_{T,\text{TES}}$	Energy (heat) taken out of the thermal energy storage (TES)
p_T	Power generated by the PV

TABLE II
BREAKDOWN OF $\mathbf{s}_t$

Component	Detail: energy consumption (kWh)	Service: FCAS
$s^{+}_{T,\text{reg}}$	curtailed for regulation	regulation *raise*
$s^{-}_{T,\text{reg}}$	increased for regulation	regulation *lower*
$s^{+}_{T,\text{fast}}$	curtailed for contingency on fast time-scale	contingency fast *raise*
$s^{-}_{T,\text{fast}}$	increased for contingency on fast time-scale	contingency fast *lower*
$s^{+}_{T,\text{slow}}$	curtailed for contingency on slow time-scale	contingency slow *raise*
$s^{-}_{T,\text{slow}}$	increased for contingency on slow time-scale	contingency slow *lower*
$s^{+}_{T,\text{delay}}$	delayed & curtailed for contingency	contingency delay *raise*
$s^{-}_{T,\text{delay}}$	delayed & increased for contingency	contingency delay *lower*

energy stored in the thermal energy storage (TES) at time T, X_T, must not exceed the thermal limits of the storage unit:

$$\underline{X} \leq X_T \leq \overline{X}, \tag{2}$$

where $\underline{X} = (\underline{X}' - \overline{\theta})C^{\text{TES}}$ and $\overline{X} = (\overline{X}' - \underline{\theta})C^{\text{TES}}$ with $\overline{X}'$ and $\underline{X}'$ being the maximum or minimum temperature of the thermal energy storage unit and C^{TES} its thermal capacitance. We have reformulated [11]'s constraints $\overline{X} = (\overline{X}' - \theta_T)C^{\text{TES}}$ and $\underline{X} = (\underline{X}' - \theta_T)C^{\text{TES}}$ as the more-conservative but time-invariant constraint (2). The electric energy stored in the battery energy system B_T at time T must not exceed the battery storage unit limits:

$$\underline{B} \leq B_T \leq \overline{B}, \tag{3}$$

where $\overline{B}$ and $\underline{B}$ are the maximum and minimum energy stored in the battery. We add the following constraint on the battery energy level to ensure continuity between days:

$$B_\tau \geq B_0. \tag{4}$$

The electric baseload demand D^{baseload}_T must be satisfied in each round:

$$x_{T,\text{baseload}} \geq D^{\text{baseload}}_T, \tag{5}$$

where we have relaxed the equality constraints into an inequality constraint. This improves the stability of our tracking level's OCO algorithm with exact penalty. A time-varying equality constraint leads to constant oscillation in the decision variable around its desired values. When using an inequality, the decision smoothly gets closer to the desired value while only taking value greater than it. From an implementation point of view, this means that building always has enough energy to supply the electric baseload. The dispatched baseload surplus is then considered as losses. Lastly, we note this relaxation should not affect the scheduling level as at the optimum, the constraints will usually be active because increasing $x_{T,\text{baseload}}$ increases the objective. In our case-study, we later observe that this constraint is always active for the scheduling level and thus $x_{T,\text{baseload}} = D^{\text{baseload}}_T$ for all T. The domestic hot water (DHW) demand D^{DHW}_T must be satisfied at each round:

$$x_{T,\text{EB}}\rho^{\text{EB}} + x_{T,\text{TES}} \geq D^{\text{DHW}}_T, \tag{6}$$

where ρ_{EB} is the electric boiler efficiency coefficient. An inequality is used in (6) to represent the ability of the building to store thermal energy. This is modeled by the difference between the left-hand and right-hand sides of (6), which models the energy stored in the TES at round T. The power generated by the building's photovoltaic panel can be curtailed. It can take on any positive value below the maximum power generated, $\overline{p}_T$. The constraint is:

$$0 \leq p_T \leq \overline{p}_T. \tag{7}$$

B. Energy balance

The energy consumption of the building must satisfy the following balance equations:

$$\begin{aligned} U_T &= x_{T,\text{export}} + x_{T,\text{HVAC}} + x_{T,\text{baseload}} + x_{T,\text{EB}} + x^{\text{c}}_{T,\text{BES}} \\ &\quad + \overline{\gamma}^{+}_{T,\text{reg}} s^{+}_{T,\text{reg}} + \overline{\gamma}^{+}_{T,\text{slow}} s^{+}_{T,\text{slow}} + \overline{\gamma}^{+}_{T,\text{fast}} s^{+}_{T,\text{fast}} \\ &\quad + \overline{\gamma}^{+}_{T,\text{delay}} s^{+}_{T,\text{delay}} \\ G_T &= x_{T,\text{import}} + Hp_T + x^{\text{d}}_{T,\text{BES}} + \overline{\gamma}^{-}_{t,\text{reg}} s^{-}_{T,\text{reg}} + \overline{\gamma}^{-}_{T,\text{fast}} s^{-}_{T,\text{fast}} \\ &\quad + \overline{\gamma}^{-}_{T,\text{slow}} s^{-}_{T,\text{slow}} + \overline{\gamma}^{-}_{T,\text{delay}} s^{-}_{T,\text{delay}} \\ U_T &= G_T \end{aligned} \tag{8}$$

where Hp_T is the energy generated during round T by the PV. The parameters $\overline{\gamma}$ represent the average ratio of rounds where services are being called by the operator.

C. Building dynamics

The third set of constraints comes from the dynamics of the building. The thermal energy loss X^{loss}_T of the TES at time T is:

$$X^{\text{loss}}_T = \frac{\left(\frac{X_T}{C^{\text{TES}}} - \theta_T\right) H}{R^{\text{TES}}}, \tag{9}$$

where R^{TES} is the thermal resistance of the thermal energy storage unit. The temperature θ_T inside the building changes according to:

$$\begin{aligned} \theta_{T+1} = \theta_T + \frac{1}{C^{\text{b}}} \Bigg(&- x_{T,\text{HVAC}}\rho^{\text{HVAC}} + (1 - \pi^{\text{int}}_T) Int_T \\ &+ (1 - \zeta^{\text{sol}}_T) Sol_T - (\theta_T - \theta^{\text{out}}_T)\frac{h}{R^{\text{b}}} \Bigg) + X^{\text{loss}}_T, \end{aligned} \tag{10}$$

where ρ^{HVAC} is the HVAC efficiency, Int_T and Sol_T are the internal and solar heat gains, π_T^{int} and ζ_T^{int} are respectively their degree of ventilation, C^{b} is the thermal capacitance, R^{b} the thermal resistance and θ_T^{out} is the ambient temperature. We fix π_t^{int}, ζ_t^{int}, Int_t and Sol_t to be constant parameters. This represents a summer setting when cooling is required. We note that the minus sign from the term $-x_{T,\text{HVAC}}\rho^{\text{HVAC}}$ is removed if a winter setting with heating is modeled. We assume in this work that the HVAC is not subject to any system constraints like cycling or ramping and that the HVAC efficiency ρ^{HVAC} is constant throughout all rounds. Note that this is not a requirement. Nonconstant efficiencies and other HVAC constraints could be incorporated through a more detailed model of the HVAC system. The thermal energy inside the TES X_T evolves according to:

$$X_{T+1} = X_T + x_{T,\text{EB}}\rho^{\text{EB}} - X_T^{\text{loss}} - D_T^{\text{DHW}}, \tag{11}$$

We neglect the losses and power consumption of hot water pumps. We note that it could be incorporated by adding a coefficient greater than one in front of D_T^{DHW}. The energy level B_T inside the battery evolves according to:

$$B_{T+1} = B_T + x_{T,\text{BES}}^{\text{c}} - \frac{x_{T,\text{BES}}^{\text{d}}}{\Phi}, \tag{12}$$

where Φ is the round trip efficiency of the battery energy storage.

The building dynamics used in this work are linear. While this could lead to deviations from the actual building's behavior (e.g. temperature), the OCO-based tracking level will not be strongly affected because it relies on observations it gets from the previous round, i.e., recent measurements. Model inaccuracies may impact the scheduling level. The scheduling level, however, is not used to make physical decisions, but rather to set targets for the tracking level.

D. Operational constraints

The last set of constraints represents the operational constraints. The operating limits of the electric boiler are:

$$\frac{H\underline{P}^{\text{EB}}}{\rho^{EB}} \leq x_{T,\text{EB}} \leq \frac{H\overline{P}^{\text{EB}}}{\rho^{EB}}, \tag{13}$$

where ρ^{EB} is the coefficient of performance of the electric boiler and $\overline{P}^{\text{EB}}$ and $\underline{P}^{\text{EB}}$ are its maximum and minimum rated power transfer. The maximum and minimum heat exchange by the TES is defined similarly:

$$H\underline{P}^{\text{EB}} \leq x_{T,\text{TES}} \leq H\overline{P}^{\text{EB}}. \tag{14}$$

The HVAC system must operate under its limits:

$$\frac{H\underline{P}^{\text{HVAC}}}{\rho^{\text{HVAC}}} \leq x_{T,\text{HVAC}} \leq \frac{H\overline{P}^{\text{HVAC}}}{\rho^{\text{HVAC}}}, \tag{15}$$

where ρ^{HVAC} is the coefficient of performance of the HVAC system and $\overline{P}^{\text{HVAC}}$ and $\underline{P}^{\text{HVAC}}$ the maximum and minimum power transfer of the cooling system. We do not consider HVAC ramping constraints in our work because loads can usually ramp up and down their consumption very quickly. Ramping constraints may be added, for example, using:

$$x_{T,\text{HVAC}} - x_{T-1,\text{HVAC}} \leq H\overline{r},$$

for $T = 2, 3, \ldots, \tau$ and where $\overline{r} \geq 0$ is the maximum ramping between two consecutive time periods. The battery energy storage is also subject to operational limits and cannot be charged and discharged at the same time:

$$0 \leq x_{T,\text{BES}}^{\text{c}} \leq H\overline{P}^{\text{BES}} i_T \tag{16}$$

$$0 \leq x_{T,\text{BES}}^{\text{d}} \leq H\underline{P}^{\text{BES}}(1 - i_T), \tag{17}$$

where $\overline{P}^{\text{BES}}$ and $\underline{P}^{\text{BES}}$ are the BES maximum and minimum power transfer and where $i_T = 1$ corresponds to charging and $i_T = 0$ to discharging the battery energy storage. All energy resources must be greater than or equal to zero:

$$x_T(n) \geq 0 \text{ for } n = 1, 2, \ldots, R. \tag{18}$$

Energy import and export are limited by the grid. This leads to the following constraints:

$$x_{T,\text{import}} \leq H\overline{I}(1 - e_T) \tag{19}$$

$$x_{T,\text{export}} \leq H\overline{E}e_T, \tag{20}$$

where $e_T = 1$ corresponds to the building exporting power and $e_T = 0$ corresponds to importing power for all $T = 1, 2, \ldots \tau$ and $H\overline{I}$ and $H\overline{E}$ are respectively the network maximum imported and exported energy during a scheduling round. Finally, the building cannot curtail and increase its energy consumption at the same time. Also, if the energy demand is to be reduced, export is not allowed. Lastly, the total provided services cannot exceed the maximum curtailment or the maximum consumption increase the building can support. This translates to the following set of constraints:

$$s_{T,\text{reg}}^{+} \leq Md_T \tag{21}$$

$$s_{T,\text{reg}}^{-} \leq M(1 - d_T) \tag{22}$$

$$s_{T,\text{fast}}^{+} \leq Md_T \tag{23}$$

$$s_{T,\text{fast}}^{-} \leq M(1 - d_T) \tag{24}$$

$$s_{T,\text{slow}}^{+} \leq Md_T \tag{25}$$

$$s_{T,\text{slow}}^{-} \leq M(1 - d_T) \tag{26}$$

$$s_{t,\text{delay}}^{+} \leq Md_T \tag{27}$$

$$s_{T,\text{delay}}^{-} \leq M(1 - d_T) \tag{28}$$

$$x_{t,\text{export}} \leq \overline{E}d_T \tag{29}$$

$$\overline{s}_T^{+} \geq s_{T,\text{reg}}^{+} + s_{T,\text{fast}}^{+} + s_{T,\text{slow}}^{+} + s_{T,\text{delay}}^{+} \tag{30}$$

$$\overline{s}_T^{-} \geq s_{T,\text{reg}}^{-} + s_{T,\text{fast}}^{-} + s_{T,\text{slow}}^{-} + s_{T,\text{delay}}^{-} \tag{31}$$

where $M > 0$ is a large scalar and where $d_T = 1$ and $d_T = 0$ respectively indicate curtailment or increase of power consumption ancillary services for all $T = 1, 2, \ldots, \tau$.

The upper bounds on the services are given by:

$$\begin{aligned}\overline{s}_T^- &= \left(\min\left\{\frac{H\overline{P}^{\text{HVAC}}}{\rho^{\text{HVAC}}}, \overline{D}_T^{\text{HVAC}}\right\} - x_{T,\text{HVAC}}\right) \\ &\quad + \left(H\overline{P}^{\text{BES}} i_T - x^{\text{c}}_{t,\text{BES}}\right) \\ &\quad + \left(\min\left\{\frac{H\overline{P}^{\text{EB}}}{\rho^{\text{EB}}}, \overline{D}_T^{\text{EB}}\right\} - x_{T,\text{EB}}\right), \\ \overline{s}_T^+ &= \left(x_{t,\text{HVAC}} - \underline{D}_T^{\text{HVAC}}\right) + x^{\text{c}}_{T,\text{BES}} + \left(x_{T,\text{EB}} - \underline{D}_T^{\text{EB}}\right),\end{aligned}$$

where

$$\begin{aligned}\overline{D}_T^{\text{HVAC}} =& \frac{1}{\rho^{\text{HVAC}}}\Bigg(- C^{\text{b}}\underline{\theta} + C^{\text{b}}\theta_T + \left(1-\pi_T^{\text{int}}\right) Int_T \\ &+ \left(1-\zeta_T^{\text{sol}}\right) Sol_T - \left(\theta_T - \theta_T^{\text{out}}\right)\frac{H}{R^{\text{b}}} + C^{\text{b}} X_T^{\text{loss}}\Bigg), \\ \underline{D}_T^{\text{HVAC}} =& \frac{1}{\rho^{\text{HVAC}}}\Bigg(- C^{\text{b}}\overline{\theta} + C^{\text{b}}\theta_T + \left(1-\pi_T^{\text{int}}\right) Int_T \\ &+ \left(1-\zeta_T^{\text{sol}}\right) Sol_T - \left(\theta_T - \theta_T^{\text{out}}\right)\frac{H}{R^{\text{b}}} + C^{\text{b}} X_T^{\text{loss}}\Bigg), \\ \overline{D}_T^{\text{EB}} =& \frac{1}{\rho^{\text{EB}}}\left(\overline{X} - X_T + D_T^{\text{DHW}} + X_T^{\text{loss}}\right), \\ \underline{D}_T^{\text{EB}} =& \frac{1}{\rho^{\text{EB}}}\left(\underline{X} - X_T + D_T^{\text{DHW}} + X_T^{\text{loss}}\right).\end{aligned}$$

Each of these quantities is computed at the end of each round.

III. Scheduling level

In this section, we present the first-level mixed-integer linear program to schedule the building's energy consumption. Let $\mathbf{w}_T \in \mathbb{R}^R$ be a weight vector. The price $\lambda_{T,i}$ of electricity on different markets averaged over a scheduling round T is used as weight. These prices are exogenous parameters and are assumed to be available prior to the corresponding time period, e.g., computed from historical data. The weight vector $\mathbf{w}_T$ is given by:

$$\begin{aligned}\mathbf{w}_T = \Big(&- \lambda_{T,\text{import}}\ \lambda_{T,\text{export}}\ \lambda^+_{T,\text{reg}}\ \lambda^-_{T,\text{reg}}\ \lambda^+_{T,\text{fast}}\ \lambda^-_{T,\text{fast}} \\ &\lambda^+_{T,\text{slow}}\ \lambda^-_{T,\text{slow}}\ \lambda^+_{t,\text{delay}}\ \lambda^+_{T,\text{delay}}\ \mathbf{0}\Big)^\top,\end{aligned}$$

where $\mathbf{0} \in \mathbb{R}^{R-S-2}$ is a vector of zeros. The weight vector is used to favor or disfavor energy export and ancillary services or energy import, respectively. When markets are favorable, the focus can be put on, for example, exporting energy at high prices or importing it at low costs. The entries of the weight vector corresponding to the building requirements' or sources of flexibility's energy variables are all zero, because requirements must always be met and are modeled as constraints. The entries of $\mathbf{w}_T$ corresponding to sources of flexibility like charging or discharging the battery energy storage are then an intermediary between both aforementioned types of variables. These energy consumption variables must be coordinated as part of the total energy consumption to minimize the cost of operating the building throughout the day.

The scheduling MILP to be solved at the beginning of the desired horizon is:

$$\begin{aligned}\min_{\substack{\mathbf{x}_T, i_T, e_T, d_T,\\ T=1,2,\ldots,\tau}} \quad & \sum_{T=1}^{\tau} \mathbf{w}_T^\top \mathbf{x}_T \\ \text{subject to} \quad & (1)-(31) \\ & i_T \in \{0,1\},\ e_T \in \{0,1\},\ d_T \in \{0,1\}.\end{aligned} \tag{32}$$

While (32) is a mixed-integer program, there are only 3τ binary variables. For example, if $\tau = 24$, there are 72 binary variables, which is within the tractable range of industrial solvers.

The scheduling level sets an energy management trajectory for the day. The real-time decisions computed by the tracking level must first satisfy the building's constraints under uncertainty and then follow the trajectory. This process can, therefore, result in deviations from the scheduled trajectory. As uncertainty grows, the realized energy trajectory will deviate more and more from the scheduled trajectory, increasing the need for tracking. This may result in a difference between the net and scheduled revenue. Conversely, if there were no uncertainty, the tracking level would be unnecessary.

IV. Tracking level

In this section, we first introduce the OCO with time-varying constraints framework. Based on this framework, we formulate the tracking level of the our two-level algorithm. The technical analysis of our proposed algorithm for OCO with time-varying constraints is then presented. We conclude this section by stating the full two-level algorithm for MES building optimization.

A. OCO

We here describe the OCO with time-varying constraints framework. Let i denote the rounds' index and I be the time horizon. Let $\mathbf{z}_i \in \mathcal{Z}$ be the decision variable at round i and $\mathcal{Z} \subseteq \mathbb{R}^n$ be set of constraints that do not vary in time. An OCO with time-varying constraints takes the form

$$\begin{aligned}\min_{\mathbf{z}_i \in \mathcal{Z}} \quad & f_i(\mathbf{z}_i) \\ \text{subject to} \quad & g_{i,j}(\mathbf{z}_i) \le 0 \text{ for } j = 1,2,\ldots J \\ & h_{i,k}(\mathbf{z}_i) = 0 \text{ for } k = 1,2,\ldots K,\end{aligned} \tag{33}$$

where $f_i : \mathbb{R}^n \mapsto \mathbb{R}$ is the differentiable convex loss function, $g_{i,j} : \mathbb{R}^n \mapsto \mathbb{R}$ are convex functions for all $j = 1,2,\ldots,J$ and $h_{j,k} : \mathbb{R}^n \mapsto \mathbb{R}$ are affine functions for all $k = 1,2,\ldots,K$, for all $i = 1,2,\ldots,I$. In OCO with time-varying constraints, $\mathcal{Z}$ models the *a priori* known time-independent constraints. $g_{i,j}$ and $h_{j,k}$ model constraints that evolve through time, which can only be observed after the current round.

The goal of the forecaster is to minimize their cumulative loss up to the time horizon I. The information about the current round is only available to the forecaster when the round ends. Hence, at each round i, the forecaster must make a decision $\mathbf{z}_i$ to minimize an unknown loss function while trying to satisfy unknown constraints.

1) Prior work on OCO with time-varying constraints: Several authors have integrated time-varying constraints into OCO by allowing constraints to be instantaneously violated, but then showing that they will be met on average [23]–[27]. Neely and Hao [23] proposed an OCO algorithm based on virtual queues and gave a static regret bound. The authors of [24] used a primal descent and dual ascent algorithm, the Modified Online Saddle-Point (MOSP), and showed that it achieves a sublinear dynamic regret bound. They also provided a sublinear bound on the dynamic fit which ensures that the constraints will be satisfied, at least on average, under certain necessary conditions. Reference [26] provided an alternate virtual queue-based algorithm in which the total violation is shown to be sublinear under different necessary conditions. In [28], a penalty term is added to the loss function to simplify the projection step and improve the computation time. However, only time-invariant constraints are covered in [28].

Our approach is novel in its use of a penalty in the objective, and in that it only requires standard OCO assumptions on variation of round optima.

2) Regret: The design tool of OCO algorithms is the regret. In this work, we consider the dynamic regret

$$\texttt{Reg}_i^d = \sum_{i=1}^{I} f_i(\mathbf{z}_i) - f_i(\mathbf{z}_i^*), \tag{34}$$

where

$$\mathbf{z}_i^* \in \arg\min_{\mathbf{z}\in\mathcal{Z}} \left\{ f_i(\mathbf{z}) \text{ s.t. } g_{i,j}(\mathbf{z}) \leq 0 \ \forall\ j, h_{i,k}(\mathbf{z}) = 0 \ \forall\ k \right\},$$

the round optimal decision in hindsight. Alternatively, in some works the static regret is used as the design tool. The static regret uses the best-fixed decision in hindsight as the comparator in the second term of the sum in (34). A bounded dynamic regret implies a bounded static regret [24] and for this reason, we only use the former. When designing an OCO algorithm, the goal is to obtain, in the worst-case, a sublinear regret in the number of rounds. A sublinear dynamic regret implies that, on average, the algorithm plays the round optimal decision in hindsight at each round [19], [29].

B. OCO-based tracking level

We now introduce the second level of our building management algorithm. We present our OCO-based algorithm for tracking the energy trajectory set by the scheduling MILP of Section III.

Let $\mathbf{u}_t \in \mathbb{R}^S$, $t = 1, \ldots, F$, be the services that are accepted but uncalled by the operator. Let $\mathbf{y}_t \in \mathbb{R}^S$, $t = 1, 2, \ldots, F$, be the services dispatched after being called. The components of both $\mathbf{u}_t$ and $\mathbf{y}_t$ are organized as in the $\mathbf{s}_T$ vector. We use q_t as the tracking round analogue of p_T for the PV generation. Let $\mathbf{z}_t \in \mathbb{R}^{R+S}$ for $t = 1, 2, \ldots, F$ be the tracking decision variable define as:

$$\mathbf{z}_t = \Big(z_{t,\text{import}} \ \ x_{t,\text{export}} \ \ \mathbf{u}_t^\top \ \ z_{t,\text{HVAC}} \ \ z_{t,\text{baseload}} \ \ z_{t,\text{EB}} \ \ z_{t,\text{BES}}^{\text{c}} \ \ z_{t,\text{BES}}^{\text{d}} \ \ z_{t,\text{TES}} \ \ q_t \ \ \mathbf{y}_t^\top \Big)^\top.$$

Finally, define

$$\overline{\mathbf{x}}_T = \Big(\mathbf{x}_T \ s_{T,\text{reg}}^+ \ s_{T,\text{reg}}^- \ s_{T,\text{fast}}^+ \ s_{T,\text{fast}}^- \ s_{T,\text{slow}}^+ \ s_{T,\text{slow}}^- \ s_{T,\text{delay}}^+ \ s_{T,\text{delay}}^- \Big)^\top,$$

for $T = 1, 2, \ldots, \tau$. In other words, an additional $\mathbf{s}_T$ vector is appended to $\mathbf{x}_T$ to form $\overline{\mathbf{x}}_T$. This is used to model called and uncalled services. Further details will be given shortly.

The objective function $o_t(\overline{\mathbf{x}}_T, \mathbf{z}_t)$ of our tracking algorithm is:

$$o_t(\overline{\mathbf{x}}_T, \mathbf{z}_t) = \sum_{r=1}^{R+S} a_{r,t} \left(\psi_{r,t}(\overline{x}_T(r)) - z_t(r) \right)^2, \tag{35}$$

for all $t = 1, 2, \ldots, F$ and for $T = 1, 2, \ldots, \tau$. In (35), $a_{r,t}$ is the tracking weight and $\psi_{r,t} : \mathbb{R} \mapsto \mathbb{R}$ is a scaling function for the requirement or service r at time t. For $r = R + 1$ to $R + S$, $\psi_{r,t}$ also indicates if the service is called or not. The function $\psi_{r,t}$ is used to scale the scheduling objective to the tracking time scale. In our case study, we use

$$\psi_{r,t}(\overline{x}_T(r)) = \begin{cases} \frac{\overline{x}_T(r)}{F} & \text{for } r = 1, 2, \ldots R \\ \frac{\gamma_{t,r}^{\pm} \overline{x}_T(r)}{F} & \text{for } r = R+1, R+2, \ldots R+S, \end{cases}$$

where $\gamma_{t,r}^{\pm} \in \{0, 1\}$ indicates if a service is called ($\gamma = 1$) or not ($\gamma = 0$). We use a weighted squared tracking error to penalize large deviations from the scheduling objective. Equivalently, we express the objective function as,

$$o_t(\overline{\mathbf{x}}_T, \mathbf{z}_t) = \left\| \boldsymbol{\psi}_t(\overline{\mathbf{x}}_T) - \mathbf{z}_t \right\|_{\mathbf{A}_t}^2, \tag{36}$$

where $\mathbf{A}_t = \text{diag}(a_{r,t} \text{ for } r = 1, 2, \ldots, R + S)$ and $\|\mathbf{v}\|_{\mathbf{A}_t}^2 = \mathbf{v}^\top \mathbf{A}_t \mathbf{v}$ is the norm induced by the matrix $\mathbf{A}_t$. Note that o_t is strongly convex if $\mathbf{A}_t$ is positive definite. In the case study, we set the tracking weight matrix $\mathbf{A}_t$ to

$$\begin{aligned} \mathbf{A}_t = \text{blockdiag}\big[&\mathbf{I} + \text{diag}(\mathbf{w}_T) - \text{diag}(\widetilde{\mathbf{w}}_t), \\ &\alpha\mathbf{I} + \text{diag}(\mathbf{w}_T[2:8]) - \text{diag}(\widetilde{\mathbf{w}}_t[2:8]) \big], \end{aligned} \tag{37}$$

for $t = 1, 2, \ldots, F$, at each T and where α is a tuning parameter. It can be used to decrease the response time to a call signal by setting it larger than 1. When α is set to values higher than one, the weight $a_{r,t}$ in the loss function (35) for the called services $\mathbf{y}_t$ will dominate the other weights and hence will lead quicker response to called services because the absolute value of gradient will take larger values. In (37), $\mathbf{w}_T$ represents the average price used in the scheduling MILP and $\widetilde{\mathbf{w}}_t$ represents the current prices. The parameter $\mathbf{w}_T$ is known prior the the tracking rounds while $\widetilde{\mathbf{w}}_t$ is observed after the tracking round. We assume that $w_T(r) - \widetilde{w}_t(r) > -1$ for all r, and thus $\mathbf{A}_t$ is positive definite for all t. This matrix is used to prioritize or deprioritize services that respectively have a higher or lower value at time t than the average used for scheduling.

Let $\mathcal{Z}_T$ be the set defined by the union of (1) – (3) and (13) – (29), where $\mathbf{x}_T$ and H have been replaced by $\mathbf{z}_t$ and h, respectively. Note that the binary variables i_T, e_T and d_T have already been fixed by the first-level algorithm and thus the parameters of $\mathcal{Z}_T$ do not change over a scheduling round

T. The tracking problem is also subject to time-dependent constraints, which we adapt from Section II:

$$\underline{D}_{t,\text{HVAC}} \leq z_{t,\text{HVAC}} \leq \overline{D}_t^{\text{HVAC}}, \tag{38}$$
$$z_{t,\text{baseload}} \geq D_t^{\text{baseload}}, \tag{39}$$
$$z_{t,\text{EB}}\rho^{\text{EB}} + z_{t,\text{TES}} \geq D_t^{\text{DHW}}, \tag{40}$$
$$q_t \leq PV_t \tag{41}$$
$$u^+_{t,\text{reg}} + u^+_{t,\text{fast}} + u^+_{t,\text{slow}} + u^+_{t,\text{delay}} \leq \overline{u}^+_t, \tag{42}$$
$$u^-_{t,\text{reg}} + u^-_{t,\text{fast}} + u^-_{t,\text{slow}} + u^-_{t,\text{delay}} \leq \overline{u}^-_t, \tag{43}$$
$$y^+_{t,\text{reg}} + y^+_{t,\text{fast}} + y^+_{t,\text{slow}} + y^+_{t,\text{delay}} \leq \overline{u}^+_t, \tag{44}$$
$$y^-_{t,\text{reg}} + y^-_{t,\text{fast}} + y^-_{t,\text{slow}} + y^-_{t,\text{delay}} \leq \overline{u}^-_t, \tag{45}$$
$$z^{\text{c}}_{t,\text{BES}} = 0 \text{ if } B_{T+t-1} = \overline{B}, \tag{46}$$
$$z^{\text{d}}_{t,\text{BES}} = 0 \text{ if } B_{T+t-1} = \underline{B}, \tag{47}$$
$$z_{t,\text{TES}} = 0 \text{ if } X_{T+t-1} = \underline{X}, \tag{48}$$
$$z_{t,\text{EB}} = 0 \text{ if } X_{T+t-1} = \overline{X}, \tag{49}$$
$$B_{T+t-1} + z^{\text{c}}_{t,\text{BES}} - \frac{z^{\text{d}}_{t,\text{BES}}}{\Phi} \geq B_0 \text{ if } T = \tau - 1, \tag{50}$$

where $\overline{u}^+_t$ and $\overline{u}^-_t$ are defined similarly to $\overline{s}^-_T$ and $\overline{s}^+_T$. Finally, D_t^{baseload}, D_t^{DHW} and PV_t are fixed values observed at the end of a round. The parameter PV_t is the tracking round analog of $\overline{p}_t$. Because OCO does not use a lookahead step, we enforce a stricter version of (4) given in (50). This constrains the BES energy level for all tracking rounds in the final scheduling round to be greater than B_0.

The tracking problem during the scheduling round T is

$$\begin{aligned}
\min_{\substack{\mathbf{z}_t \in \mathcal{Z}_T \\ \text{for } t=1,2,\ldots,F}} \quad & \sum_{t=1}^{F} \|\boldsymbol{\psi}_t(\overline{\mathbf{x}}_T) - \mathbf{z}_t\|^2_{\mathbf{A}_t} \\
\text{subject to} \quad & (38) - (50) \text{ for all } t = 1, 2, \ldots, F. \\
& U_t = z_{t,\text{export}} + z_{t,\text{HVAC}} + z_{T,\text{baseload}} + z_{t,\text{EB}} \\
& \quad + z^{\text{c}}_{t,\text{BES}} y^+_{t,\text{reg}} + y^+_{t,\text{slow}} + y^+_{t,\text{fast}} + y^+_{t,\text{delay}} \\
& G_t = z_{t,\text{import}} + q_t + z^{\text{d}}_{t,\text{BES}} + y^-_{t,\text{reg}} + y^-_{t,\text{fast}} \\
& \quad + y^-_{t,\text{slow}} + y^-_{t,\text{delay}} \\
& U_t = G_t \text{ for all } t = 1, 2, \ldots, F.
\end{aligned}$$

where the information for round t is only observed when the current round ends. We solve this problem using the OGD with exact penalty presented in (55) and in Corollary 1 of Section IV-C. The exact penalty function for the tracking algorithm is provided in (51) in which $[b]^+ = \max\{0, b\}$ and the indicator function $\mathbb{I}_b = 1$ if b is true and $\mathbb{I}_b = 0$ otherwise. The OCO with exact penalty is given by

$$\min_{\mathbf{z}_t \in \mathcal{Z}_T} \|\boldsymbol{\psi}_t(\overline{\mathbf{x}}_T) - \mathbf{z}_t\|^2_{\mathbf{A}_t} + cP_t(\mathbf{z}_t), \tag{52}$$

where $c > 0$ is set according to Theorem 1. We denote the objective function of (52) as $f_{T,t}(\mathbf{x}_T, \mathbf{z}_t)$. Note that because the first term of $f_{T,t}(\mathbf{x}_T, \mathbf{z}_t)$ is strongly convex, so is $f_{T,t}(\mathbf{x}_T, \mathbf{z}_t)$.

For the OGD with exact penalty update, we use a subgradient of the loss function. A subgradient of the penalty function, P'_t, is given by:

$$P'_t = \sum_{j=1}^{J} \nabla g_j(\mathbf{z}_t)\mathbb{I}_{g_j(\mathbf{z}_t)>0} + \sum_{k=1}^{K} \text{sign}(h_k(\mathbf{z}_t))\nabla h_k(\mathbf{z}_t).$$

The following is then a subgradient of the loss function:

$$\nabla f_{T,t}(\mathbf{x}_T, \mathbf{z}_t) = 2\mathbf{A}_t\left(\mathbf{z}_t - \boldsymbol{\psi}_t(\overline{\mathbf{x}}_T)\right) + cP'_t.$$

C. Theoretical analysis of OCO with exact penalty

The OCO with exact penalty framework is a minor extension of existing frameworks for OCO with time-varying constraints. In this subsection, we prove that our algorithm for the OCO with exact penalty framework achieves sublinear regret.

We first introduce some notation and the assumptions we will be using to in this work. In this subsection, we index the OCO rounds $i = 1, 2, \ldots, I$. We define the cumulative variation term V_I and cumulative constraint variation term $V_I^{\mathbf{g}}$ as:

$$V_I = \sum_{i=2}^{I} \left\|\mathbf{z}^*_i - \mathbf{z}^*_{i-1}\right\|,$$
$$V_I^{\mathbf{g}} = \sum_{i=2}^{I} \max_{\mathbf{z}\in\mathcal{Z}} \left\|[\mathbf{g}_i(\mathbf{z}) - \mathbf{g}_{i-1}(\mathbf{z})]^+\right\|,$$

where $[\mathbf{y}]^+$ returns the vector $\mathbf{v} \in \mathbb{R}^n$ were $v(m) = \max\{0, y(m)\}$ for $m = 1, 2, \ldots, n$. These terms represent the variation in the optimal solutions and the changes of the feasible set size. We don't make use of the constraint variation term in our analysis. We only define it for future comparison with the literature.

We now list our assumptions. These assumption are standard in the OCO literature [18], [19].

A.1) The decision variable $\mathbf{z}_i \in \mathcal{Z}$ for all $i = 1, 2, \ldots, I$, where $\mathcal{Z}$ is a convex and compact set.
A.2) The loss function is B-bounded: $\|f_i(\mathbf{z}_i)\| \leq B$ for $i = 1, 2, \ldots, I$.
A.3) The gradient of the loss function is G-bounded: $\|\nabla f_i(\mathbf{z}_i)\| \leq G$ for $i = 1, 2, \ldots, I$.

As a consequence of A.1, the decision variable is also Z-bounded: $\|\mathbf{z}_i\| \leq Z$ for $i = 1, 2, \ldots, I$.

We show that using a ℓ_1-exact penalty, we can solve an OCO problem with a time-varying feasible set without the need to characterize its variation.

Definition 1 (ℓ_1-exact penalty function)**.** *Let $P : \mathbb{R}^R \mapsto \mathbb{R}$ be the ℓ_1-exact penalty function defined as:*

$$P_i(\mathbf{z}_i) = \sum_{j=1}^{J} [g_{i,j}(\mathbf{z}_t)]^+ + \sum_{k=1}^{K} |h_{i,k}(\mathbf{z}_t)|,$$

We first shown the following lemma and then use it in the main technical result of Theorem 1.

Lemma 1 (Penalized problem)**.** *Suppose that the constrained program* (33) *is primal and dual feasible at time i and let*

$$
\begin{aligned}
P_t(\mathbf{z}_t) = &\left[\underline{D}_t^{\text{HVAC}} - z_{t,\text{HVAC}}\right]^+ + \left[z_{t,\text{HVAC}} - \overline{D}_t^{\text{HVAC}}\right]^+ + \left[D_t^{\text{baseload}} - z_{t,\text{baseload}}\right]^+ + \left[D_t^{\text{DHW}} - z_{t,\text{EB}}\rho^{\text{EB}} - z_{t,\text{TES}}\right]^+ \\
&+ \left[q_t - PV_t\right]^+ + \left[u_{t,\text{reg}}^+ + u_{t,\text{fast}}^+ + u_{t,\text{slow}}^+ + u_{t,\text{delay}}^+ - \overline{u}_t^+\right]^+ + \left[u_{t,\text{reg}}^- + u_{t,\text{fast}}^- + u_{t,\text{slow}}^- + u_{t,\text{delay}}^- - \overline{u}_t^-\right]^+ \\
&+ \left[y_{t,\text{reg}}^+ + y_{t,\text{fast}}^+ + y_{t,\text{slow}}^+ + y_{t,\text{delay}}^+ - \overline{u}_t^+\right]^+ + \left[y_{t,\text{reg}}^- + y_{t,\text{fast}}^- + y_{t,\text{slow}}^- + y_{t,\text{delay}}^- - \overline{u}_t^-\right]^+ \\
&+ \mathbb{I}_{B_{T+t-1}=\underline{B}}|z_{t,\text{BES}}^d| + \mathbb{I}_{B_{T+t-1}=\overline{B}}|z_{t,\text{BES}}^c| + \mathbb{I}_{X_{T+t-1}=\overline{X}}|z_{t,\text{EB}}| + \mathbb{I}_{X_{T+t-1}=\underline{X}}|z_{t,\text{TES}}| \\
&+ \mathbb{I}_{T=\tau-1}\left[B_0 - B_{T+t-1} - z_{t,\text{BES}}^{\text{c}} + \frac{z_{t,\text{BES}}^{\text{d}}}{\Phi}\right]^+.
\end{aligned} \tag{51}
$$

$\mathbf{x}_i^{*,\text{constrained}}$ *be its the optimum. Define the penalized optimization problem as*

$$\min_{\mathbf{z}_i \in \mathcal{Z}} f_i(\mathbf{z}_i) + cP_i(\mathbf{z}_i), \tag{53}$$

and denote its optimum by $\mathbf{z}_i^{*,\text{penalized}}$*. If* f_i *is strongly convex and* $c > \left\|(\boldsymbol{\lambda}_i^* \;\; \boldsymbol{\nu}_i^*)^\top\right\|_\infty$ *where* $\boldsymbol{\nu}_i^*$ *and* $\boldsymbol{\lambda}_i^*$ *are the optimal dual variables of the constrained program* (33)*, then* $\mathbf{z}_i^{*,\text{penalized}} = \mathbf{z}_i^{*,\text{constrained}}$.

Proof. Because f_i is strongly convex, the objective function of (53) is also strongly convex and thus strictly convex. Therefore, the set of minimizers of (53) is a singleton. It then follows from [30, Theorem 17.3] that $\mathbf{z}_i^{*,\text{penalized}} = \mathbf{z}_i^{*,\text{constrained}}$. □

Theorem 1 (OCO with ℓ_1-exact penalty)**.** *Suppose that all assumptions of Lemma 1 hold. Then any OCO algorithm that achieves sublinear regret with a time-invariant feasible set will also achieve sublinear regret on* (53)*. Thus, the algorithm plays, at least on average, round optimal decisions which are feasible for the original problem,* (33)*.*

Proof. Let $\mathcal{A}_\mathcal{Z}$ be an OCO algorithm for time-invariant feasible set $\mathcal{Z}$ such that $\texttt{Reg}_I^d(\mathcal{A}_\mathcal{Z}) < O(I)$. First, observe that the penalized optimization problem (53) has a time-invariant feasible set. We can therefore apply $\mathcal{A}_\mathcal{Z}$ to sequentially solve (53). Denote by $\mathcal{A}_\mathcal{Z}^p$ the algorithm $\mathcal{A}_\mathcal{Z}$ applied to the penalized problem (53).

Let $\mathbf{z}_i^{*,\text{penalized}}$ be the optimum of (53) and $\mathbf{z}_i^{*,\text{constrained}}$ be the solution of (33) at time i. The regret of $\mathcal{A}_\mathcal{Z}^p$ is given by,

$$\texttt{Reg}_I^d(\mathcal{A}_\mathcal{Z}^p) = \sum_{i=1}^I f_i(\mathbf{z}_i) - f_i(\mathbf{z}_i^{*,\text{penalized}}). \tag{54}$$

By Lemma 1, we have $\mathbf{z}_i^{*,\text{penalized}} = \mathbf{z}_i^{*,\text{constrained}}$ for all i. We can re-express (54) as

$$\texttt{Reg}_I^d(\mathcal{A}_\mathcal{Z}^p) = \sum_{i=1}^I f_i(\mathbf{z}_i) - f_i(\mathbf{z}_i^{*,\text{constrained}}) < O(I),$$

where the last inequality follows from the assumption $\texttt{Reg}_I^d(\mathcal{A}_\mathcal{Z}) < O(I)$. Consequently, since $\frac{\texttt{Reg}_I^d(\mathcal{A}_\mathcal{Z}^p)}{I} \to 0$ as I increases, the forecaster plays, at least on average, the optimum of the time-varying constrained problem (33). By definition, the optimum of (33) is feasible and it follows that the decision played by $\mathcal{A}_\mathcal{Z}^p$ will be, at least on average, a feasible point of the time-varying constraints. □

We now present the OCO algorithm we use in the tracking level of our approach. Consider the online gradient descent (OGD) proposed by [31]. In round i, the decision in round $i+1$ is given by:

$$\mathbf{z}_{i+1} = \operatorname*{proj}_\mathcal{Z}\left(\mathbf{z}_i - \eta \nabla f_i(\mathbf{z}_i)\right), \tag{55}$$

where $\text{proj}_\mathcal{Z}\,\mathbf{y} \in \arg\min_{\mathbf{z}\in\mathcal{Z}} \|\mathbf{z} - \mathbf{y}\|$ is the projection operator and η, the descent step size, is set to be inversely proportional to $\sqrt{I}$.

Corollary 1 (OGD with exact penalty)**.** *Suppose we apply* OGD *to* (53) *and that* f_i *and* c *satisfy the assumptions of Theorem 1. Then*

$$\texttt{Reg}_I^d \leq \left(\frac{7Z^2}{4\chi} + \frac{\chi G^2}{2} + \frac{ZV_I}{\chi}\right)\sqrt{I},$$

where χ *is a positive scalar. Equivalently we have* $\texttt{Reg}_I^d \leq O\left(\sqrt{I}\,(1+V_I)\right)$.

Proof. The result follows from applying OGD with $\eta = \chi I^{-1/2}$ to (53). □

Corollary 1 implies a stricter constraint on V_I when compared to the MOSP algorithm [24]. We note that any OCO algorithm can be used in pair with the exact penalty of Theorem 1. Thus using a different algorithm may lead to a looser constraint on V_I and an improved bound.

Our approach has two main advantages. First, it does not constrain the set variation $V_I^\mathbf{g}$, unlike [24]'s and [26]'s algorithms. With our approach, V_I suffices to capture the variation of the time-varying feasible set and round optimum. The second gain is that the algorithm is not constrained by the dynamic fit for the constraint satisfaction [23], [24], [27]. As showed in Theorem 1, the penalty-based update directly ensures that the constraints are satisfied when the regret is sublinearly bounded above.

We note that minimal assumptions are made about the sequence of loss functions $\{f_i\}_{i=1}^I$. This sequence can therefore be stochastic, deterministic or even adversarial and still lead to a bounded regret. This implies that, for any realization of the uncertainty, Theorem 1 and Corollary 1 hold, and the tracking algorithm will output at least on average the round optimal decision.

D. Two-level algorithm

The full two-level algorithm is given in Algorithm 1.

Algorithm 1 Two-level MES building real-time optimization algorithm

Parameters: Historical data/predictions for $\mathbf{w}_T$ and (1) – (31), $\chi > 0$,$\eta = \chi/\sqrt{T}$ and c.

Level 1:

Solve Scheduling MILP:

$$\{\mathbf{x}_T, i_T, e_T, d_T\}_{T=1}^{\tau} = \underset{\substack{\mathbf{x}_T, i_T, e_T, d_T, \\ T=1,2,\ldots,\tau}}{\arg\min} \quad \mathbf{w}_T^\top \mathbf{x}_T$$

$$\text{subject to} \quad (1)-(31)$$

$$i_T \in \{0,1\},$$

$$e_T \in \{0,1\}$$

$$d_T \in \{0,1\}$$

Level 2:

for $T = 1, 2, \ldots, \tau$ **do**

  Initialization: $\mathbf{z}_0 = \mathbf{0}$

  for $t = 1, 2, \ldots, F$ **do**

    Schedule the building energy usage and services according to $\mathbf{z}_t$.

    Observe outcome of the round.

    Calculate the gradient $\nabla f_{T,t}(\mathbf{x}_T, \mathbf{z}_t)$.

    Compute $\mathbf{z}_{t+1} = \text{proj}_{\mathcal{Z}_T}(\mathbf{z}_t - \eta \nabla f_{T,t}(\mathbf{x}_T, \mathbf{z}_t))$.

    Dispatch $\mathbf{z}_{t+1}$.

  end for

end for

TABLE III
BUILDING PARAMETERS (*'*' indicates fixed values)*

	Definition	Value	Source
C^{b}	Building thermal capacitance	19.33 kWh/°C	[35], [36]
R^{b}	Building thermal resistance	10.80°C/kW	[35], [36]
θ_{d}	Desired temperature	21°C	[37]
$\overline{\theta}$	Maximum temperature	20°C	[37]
$\underline{\theta}$	Minimum temperature	22°C	[37]
ρ^{HVAC}	HVAC efficiency	2.5	[37]
$\overline{P}^{\text{HVAC}}$	Maximum rated power	14 kW	[37]
$\underline{P}^{\text{HVAC}}$	Minimum rated power	0 kW	*
α	Blind exclusion efficiency	0.47	[11]
Sol	Solar heat gain	0.005 kWh	*
ζ	Sol degree of ventilation	0.5α	*
Int	Internal heat gain	0 kWh	*
π	Int degree of ventilation	0.3	*
$\overline{X}$	TES maximum temperature	80°C	[8]
$\underline{X}$	TES minimum temperature	55°C	[8]
C^{TES}	TES thermal capacitance	0.3483 kWh/°C	[8]
R^{TES}	TES thermal resistance	567 kWh/°C	[8]
ρ^{EB}	EB efficiency	0.9	[11]
$\overline{P}^{\text{TES}}$	TES maximum power	1.5 kW	*
$\underline{P}^{\text{TES}}$	TES minimum power	0 kW	*
$\overline{B}$	BES maximum capacity	13.5 kWh	[38]
$\underline{B}$	BES minimum capacity	0 kWh	*
$\overline{P}^{\text{BES}}$	BES maximum power	5 kW	[38]
$\underline{P}^{\text{BES}}$	BES minimum power	0 kW	*
Φ	BES round trip efficiency	0.9	[38]
$\overline{I}$	Maximum energy import	4.94 kW	[11]
$\overline{E}$	Maximum energy export	4.94 kW	[11]
$Area$	PV panel area	20 m^2	*
Φ^{PV}	PV efficiency	0.222	[39]
PR	PV performance ratio	0.85	[40]

V. CASE STUDY

We apply the two-level algorithm to a case-study based on a terraced building in Melbourne, Australia. We use `CVXPY` [32] with the `Gurobi` solver [33] for the scheduling MILP, and with the `ECOS` [34] solver for projection steps of the OCO algorithm.

A. Setting

The building's parameters are listed in Table III. The electric baseload demand and domestic hot water demand are based on United Kingdom data [11], [35], [36]. The ambient temperature and solar irradiance are taken from [41] for a Summer day for the region of Melbourne, Victoria, Australia. The electricity retail import and export prices of the state of Victoria are from [42]. The FCAS prices are taken form [43]. Let $H = 1$ hour, $\tau = 24$, $h = 0.5$ minute and $F = 120$. We set $\theta_0 = 21$°C, $X_0 = 15$ kWh and $B_0 = 5.0$ kWh. We set the numerical parameter χ to 0.1 and $\alpha = 5$. We use Monte Carlo simulations to estimate an upper bound on the tracking problem dual variables for any realization of the uncertainty. We set $c = 3.0$. We linearly interpolate all demand, environment and price data to compute their respective values for each 0.5 minute rounds.

All time-varying data are subject to Gaussian noise to model uncertainty. Truncated Gaussian variables with standard deviations computed from historical data are used for all parameters except for the temperature and the prices. The standard deviation of the temperature is scaled down by a factor of 50 because it does not vary significantly over a half minute interval. The standard deviation of the prices is set to 0.01, i.e., the equivalent of \$0.01. The decision $\gamma_{t,s}^{\pm}$ of an operator to call a service or not is modeled by independent and identically distributed Bernoulli random variables with probability β for each service and each tracking rounds. Note that $\gamma_{t,s}^{\pm} = 1$ to indicate if a service is called and 0 otherwise. The value of the decision is kept to 1 for the total duration of the service, e.g., for 10 rounds in the case of contingency slow services, after which it is re-sampled. In the case of delay contingency, it is kept to 1 for 10 minutes and then re-sample. We set $\beta = 0.2$ and $\overline{\gamma}_{T,s}^{\pm} = 0.4$ for all services. To emphasize on the adaptability of the real-time level, $\overline{\gamma}_{T,s}^{\pm}$ is set to differ from the actual average ratio of rounds the service are called.

Because the tracking rounds in our case study are 0.5 minutes, we only consider slow contingency services. For fast contingency services, the tracking round size must be decreased below ten seconds as the response time of the loads must be within six seconds [12].

B. Numerical results

1) Scheduling level: First, we give an example of the output of the first level of the algorithm for a day. The plan produced by the scheduling level has a net revenue of \$4.60, including any expenses due to electricity import. The energy used for requirements and services are presented in Figures 2 and 3 respectively. A discussion of the outcome of is provided in the following section.

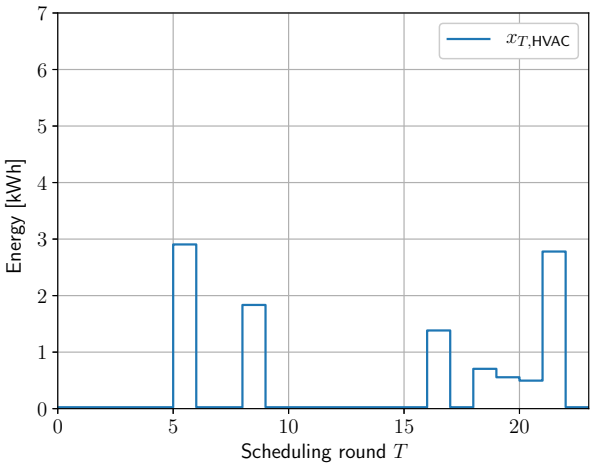

(a) HVAC

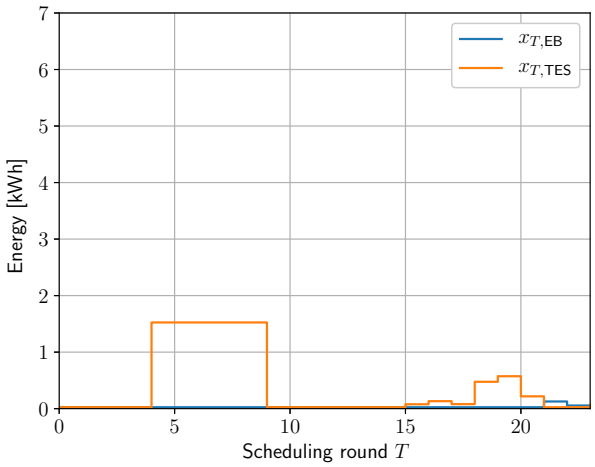

(b) EB and TES

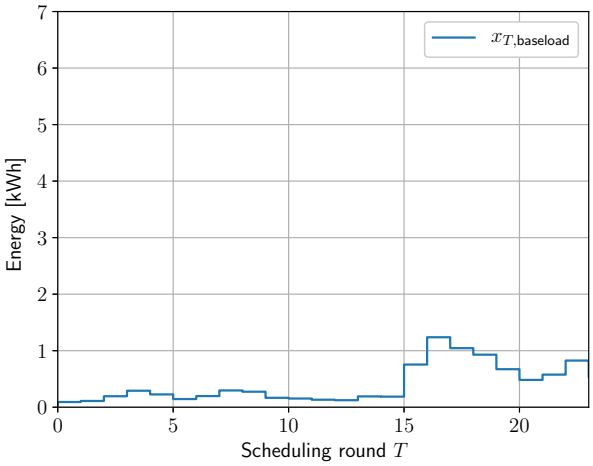

(c) Baseload

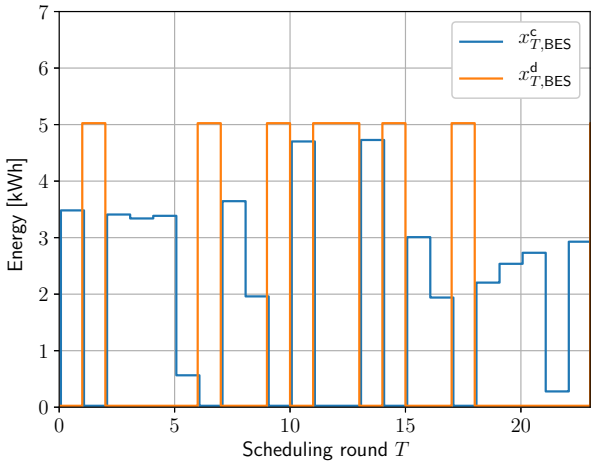

(d) BES

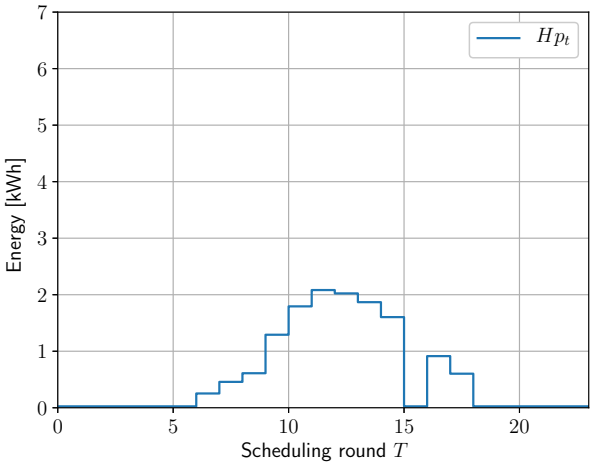

(e) Solar generation

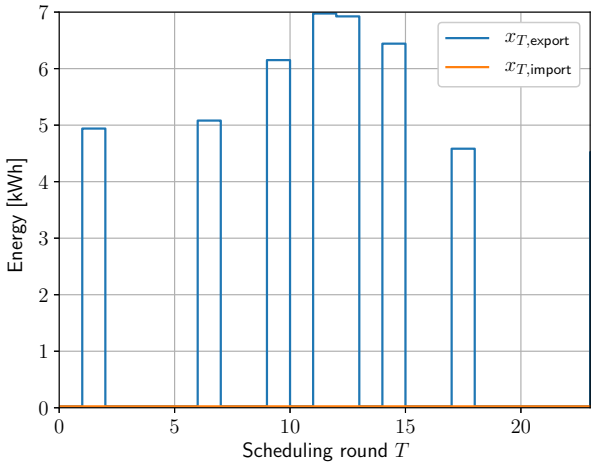

(f) Import and export

Fig. 2. Scheduled energy resources distribution for a day

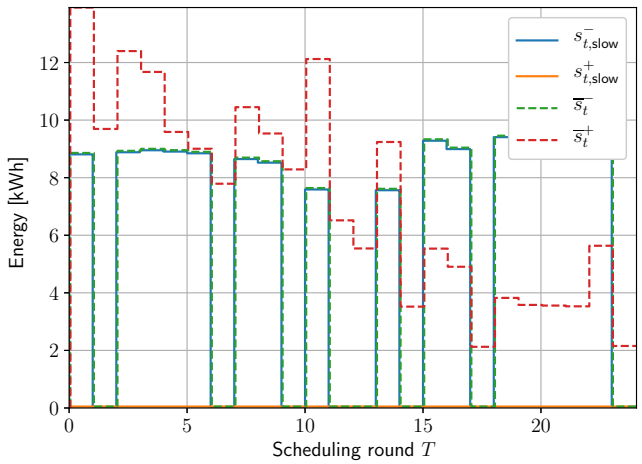

Fig. 3. Scheduled ancillary services (note: $s_{t,\text{slow}-}$ and $\overline{s}^-_T$ coincidence at all points)

2) Two-level algorithm example: We now discuss the output of the two-level algorithm. The real-time energy dispatch and the scaled and scheduled energy trajectory are presented on Figure 4. The real-time called and uncalled services are presented on Figure 5. We note the similarities of the real-time energy dispatch with the scheduled energy consumption of Figures 2 and 3, which highlights the performance of our two-level algorithm. The net revenue of the building under uncertainty is \$1.79. The discrepancy between the planned and observed net revenue can be explained by the major difference between the mean data used for the scheduling level and the real-time level.

In Figures 4 and 5 and all the following figures, the curves are not smooth. There are two reasons for this. First, the algorithm has to deal with services being intermittently called and stopped. Each time a service is called or stopped, the algorithm has to re-balance the building's generation and consumption. For example, this can be due increase consumption contingency service being called for 5 minutes. The algorithm can then increase the energy sent to the electric boiler or BES charging while ensuring all constraints are met, leading to jumps in $z_{t,\text{EB}}$ and $z^{\text{c}}_{t,\text{BES}}$. This is also observed when an MPC tracking algorithm is implemented (see Figure 9 of Section V-C). The second reason for the non-smoothness of the curves is the penalty function algorithm. Each time the prediction violates a constraint, the prediction is pushed back to the interior of the feasible set leading to another local peak. This again requires re-balancing of the buildings generation and consumption.

In Figure 6, the temperature, BES energy level and TES energy level are shown. We remark that these constraints are satisfied at almost all time. Figure 6a shows that the two-level algorithm maintains low temperature and pre-cools the unit before the high ambient temperature. At this time, it is at the mid-point of its temperature dead-band and can therefore bid on increased consumption contingency services. This has a two-fold benefit: (i) it increases the income of the unit and (ii) when called, the algorithm services energy to the HVAC unit. This process is also repeated later during the day. This can be seen by the high values of the HVAC curve in Figures 4 and 5 for the called and uncalled ancillary services. The algorithm exploits the lower import rate at the beginning time of the day to balance its energy consumption when no ancillary services are offered.

Figure 5 shows each ancillary service and the associated upper limit. Figure 5a shows the energy that is committed to each ancillary service but not called by the system operator. Figure 5b presents the called services which directly influence the energy balance of the building.

The algorithm uses the same contingency service to charge its BES and TES (via the electric boiler) shown on Figures 6b and 6c. Charging the BES is the main source of flexibility at the end of the day because the TES and temperature are close to their upper bounds. The BES can be discharged at most times because it does not rely on exogenous phenomena like hot water demand for the TES. For this reason, the BES cycles through its full capacity. When it reaches a high state of charge, the algorithm exports the energy in the BES as seen in Figure 4d. This differs from the TES, which can only provide flexibility until it reaches its maximum energy level as shown in Figure 6c. It must then wait for the building user to consume hot water to decrease its energy level. When solar energy is available to the building, we observe large energy export. Around midday, the export is higher than the discharge as the solar energy can satisfy the building's requirements.

Lastly, we show how the real-time algorithm is able to meet the MES requirements. Figure 7 shows the upper limits and dispatch of the PV, domestic hot water demand, and baseload demand for scheduling rounds 11 to 14. Figure 7a shows that the solar power generated by the PV is almost always below the maximum generation. We note that the difference between the curves in Figure 7a represents the curtailed solar generation by the building. Figure 7b shows that the energy used by the electric boiler added to the energy taken out of the TES nearly always satisfy the domestic hot water requirement. Finally, Figure 7c shows that the energy dispatched to the baseload also almost always exceeds the baseload requirements.

Finally, we run the simulation over a 45-day data set and compute the ratio of rounds in which the time-varying constraints are satisfied and the net revenue after each day. Table IV presents the ratio of tracking rounds in which the specified time-varying constraint is satisfied over the total number of tracking rounds. The overall average time-varying constraint satisfaction rate is 97.32%. These results show the high performance of OCO in uncertain, dynamic settings. The tracking rounds have a very small duration (30 seconds) and hence the 2.68% of tracking rounds with constraint violations is a relatively short time period. Because the OCO algorithm penalizes decision variables that lead to constraint violations, the rounds with violated constraints should be distributed over time. This is observed in Figure 7, in which constraint violations rarely occur in consecutive rounds. Constraint tightening strategies could be used to ensure a near perfect tracking round satisfaction rate. This is a topic for future research. We remark that violating mathematical constraints does not mean actual physical constraints will be violated. In practice, the building could be allowed to modify its energy import and export to

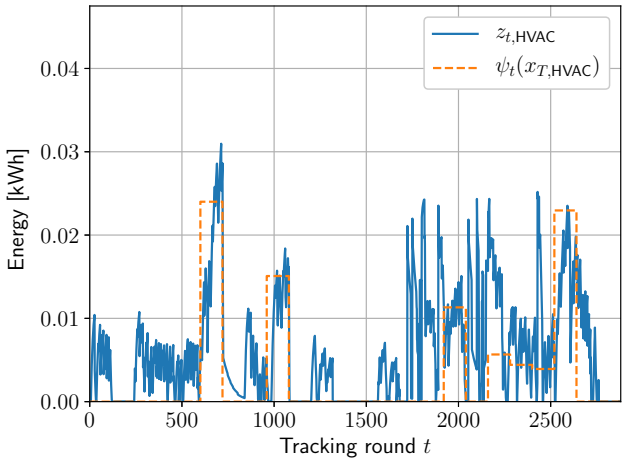

(a) HVAC

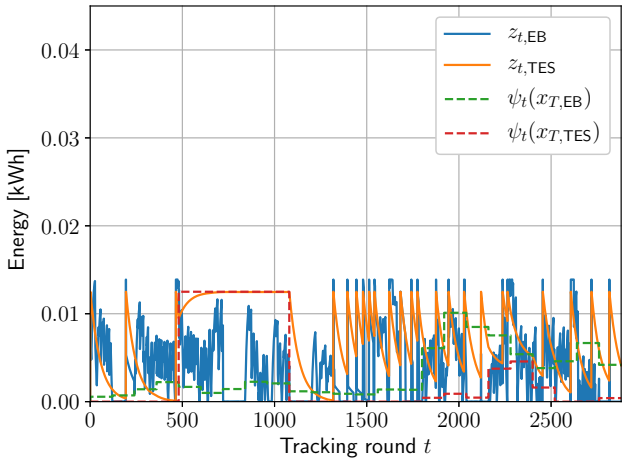

(b) EB and TES

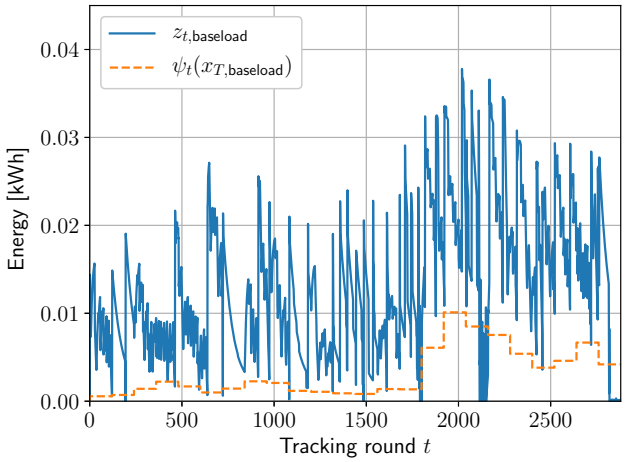

(c) Baseload

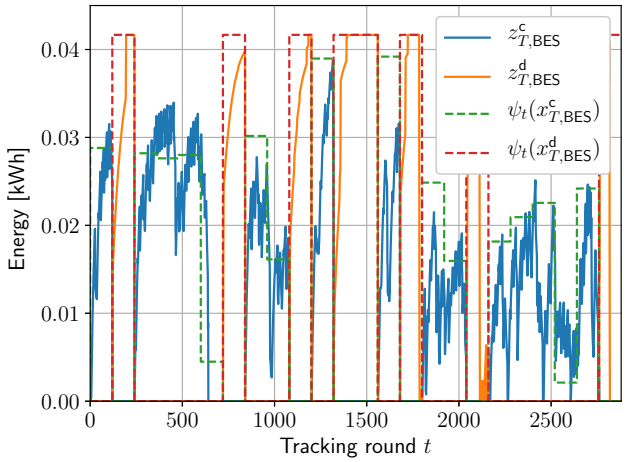

(d) BES

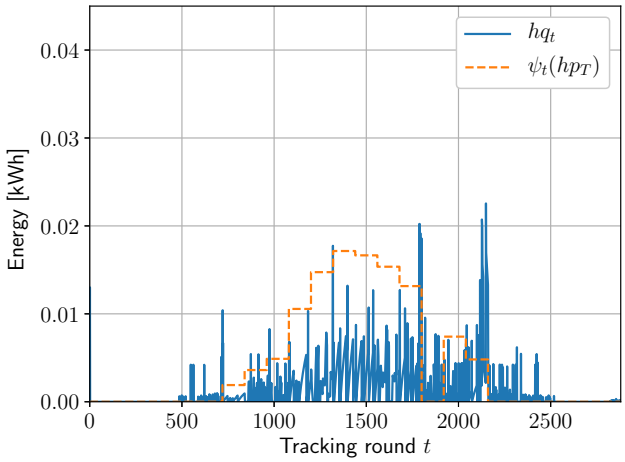

(e) Solar generation

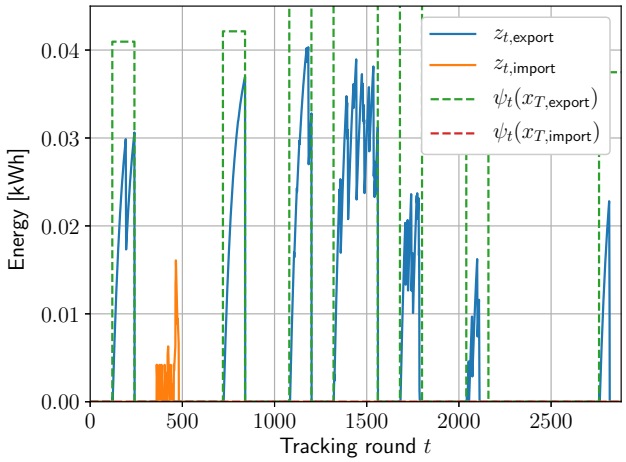

(f) Import and export

Fig. 4. Real-time energy dispatch and scheduled energy trajectory for a whole day

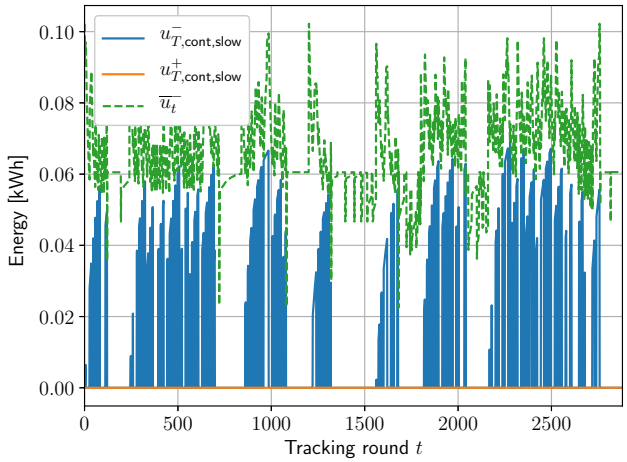

(a) Non-called services

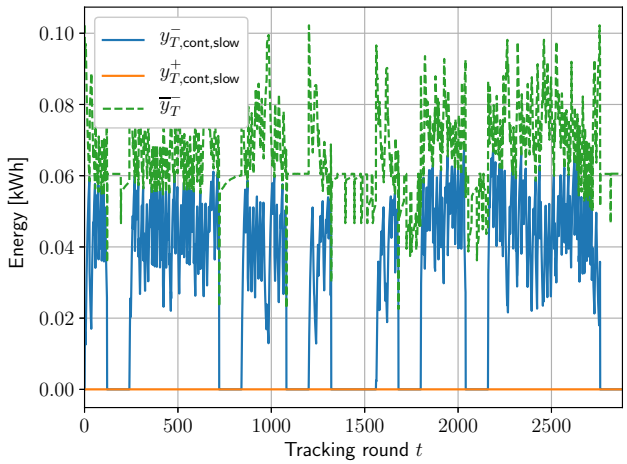

(b) Called services

Fig. 5. Real-time ancillary services dispatch and their maximum value

TABLE IV
RATIO OF TRACKING ROUNDS IN WHICH TIME-VARYINGS CONSTRAINT ARE SATISFIED OVER THE TOTAL NUMBER OF TRACKING ROUNDS (TOLERANCE 10^{-8})

Constraints	Satisfaction rate
Temperature	99.12%
BES	96.79%
TES	99.78%
PV	92.63%
DHW	99.39%
Baseload	96.19%

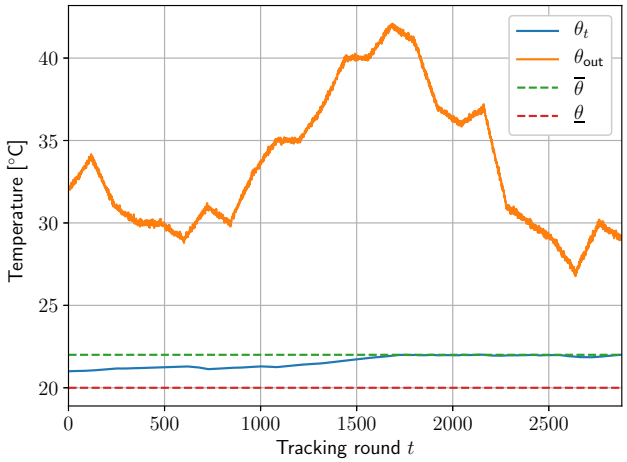

(a) Building's temperature

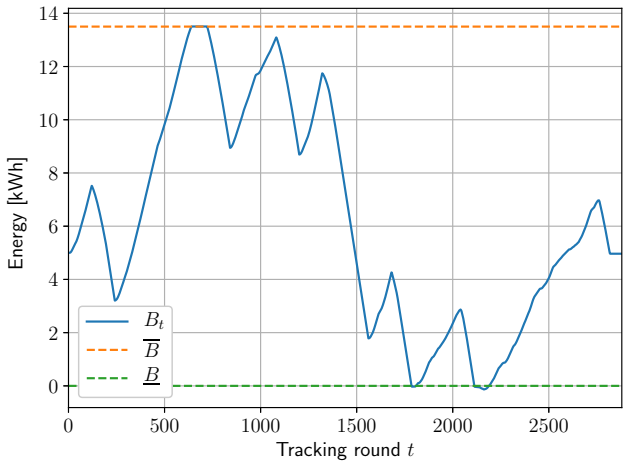

(b) Battery energy storage

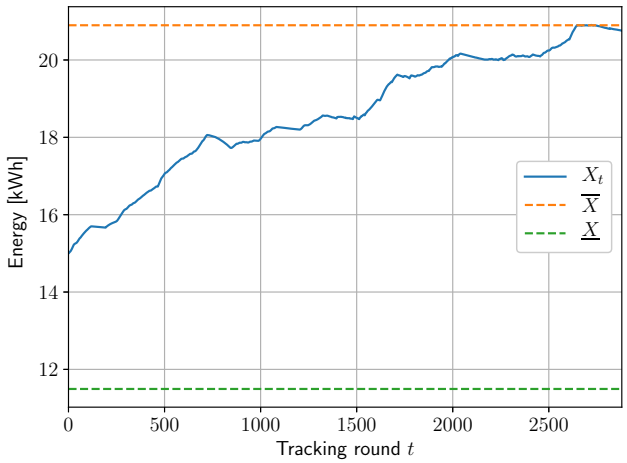

(c) Thermal energy storage

Fig. 6. Real-time energy dispatch of the building's different energy storages

avoid any imbalances. The only consequence for the building would then be a change in net revenue.

Figure 8 shows the net revenue of the building for each different day. We assumed the building has communication, control and metering abilities. The net revenue presented here does not account for the associated costs. The average net revenue is \$2.03. This is a significant improvement as the MES building net revenue would be on average $-$\$1.62 if no energy management was done, i.e. if the building was only satisfying its current needs without coordinating the available sources

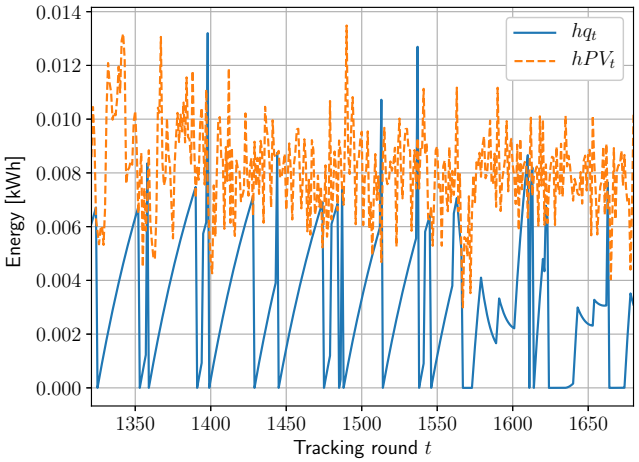

(a) Solar generation $q_t \leq PV_t$

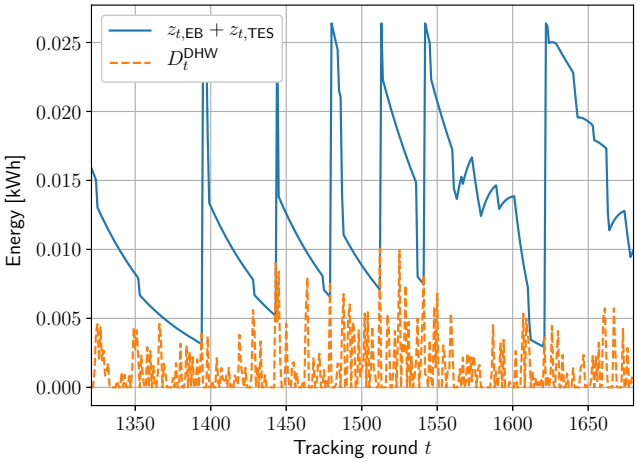

(b) DHW demand $z_{t,\text{EB}} + z_{t,\text{TES}} \geq D_t^{\text{DHW}}$

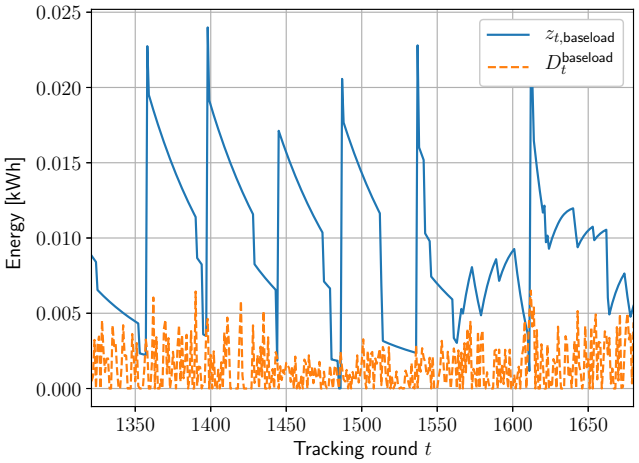

(c) Baseload $z_{t,\text{baseload}} \geq D_t^{\text{baseload}}$

Fig. 7. Real-time energy usage and their respective constraints for scheduling rounds 11 to 14

of flexibility. This shows that under unknown and noisy exogenous factors like the natural phenomena and domestic

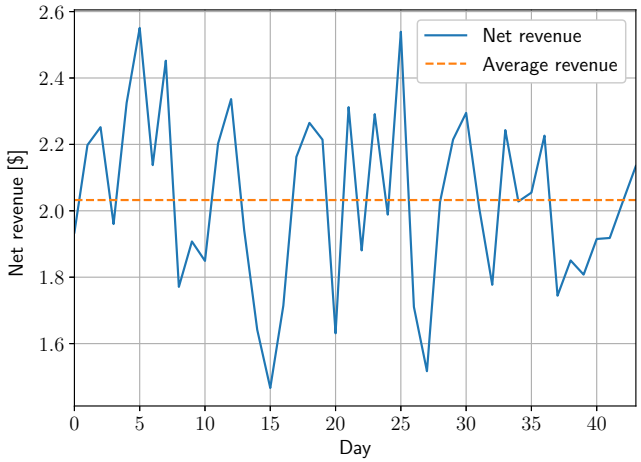

Fig. 8. Building's net revenue when using our two-level approach over a 45-day period

requirements, our proposed two-level algorithm can efficiently manage the energy resources of building-based MES.

C. Discussion: model predictive control

MPC shares some common features with OCO and could also be used in the real-time tracking level. The MPC framework assumes knowledge of future parameters, which it uses in the receding horizon computation. On the other hand, the OCO relies only on past and present information. In our two-level algorithm, only approximate information about the future is used in the scheduling level. This makes our approach amenable to a wider range of settings, e.g., outside of major metropolitan regions where extensive data may not be available.

MPC typically outperforms OCO because an optimization problem is fully solved in each round. Note that regret bounds of OCO algorithms ensure that the OCO predictions are round optimal at least on average. The trade-off is that MPC is more computationally demanding because it must solve a multi-period optimization problem in each round. In comparison, OCO only requires an algebraic operation (sum) and a projection for its update. This difference in computational cost is a limiting factor when, for example, several buildings are considered with short tracking rounds. Because of its low information needs, low computational cost and the theoretical performance guarantee, we favor OCO over MPC for large problems such as ours.

For comparison purposes, we now discuss how MPC could be applied to our problem. Let $\mu \in \mathbb{N}$ be the length of the receding horizon. At each tracking round t, we solve the receding horizon quadratic program:

$$\min_{\substack{\mathbf{z}_{t+k} \\ k=1,2,\ldots,\mu}} \quad \sum_{k=1}^{\mu} \|\boldsymbol{\psi}_{t+k}(\overline{\mathbf{x}}_T) - \mathbf{z}_{t+k}\|^2_{\mathbf{A}_t}$$

subject to $(1)-(31)$ at $t+k$ for $k = 1, 2, \ldots, \mu$

$\theta_t, B_t, X_t, X_t^{\text{loss}}$ are the observed state at t

$+$ models for $\theta_t^{\text{out}}, D_t^{\text{baseload}}, D_t^{DHW}, PV_t, \boldsymbol{\lambda}_t,$

TABLE V
COMPARISON BETWEEN THE COMPUTATION TIME REQUIRED FOR AN OCO-BASED AND MPC-BASED TRACKING LEVEL

Tracking algorithm	Average time for a day [s]	Average time per iteration [s]	Ratio of round necessiting > 30s
OCO	162	0.05	0%
MPC	73,548	25.5	13.36%

and implement the decision $\mathbf{z}_{t+1}$. The focus of this work is the use of online convex optimization in a tracking context with low information requirement. We use the present implementation because our objective is a basic qualitative comparison between OCO and MPC, and not to determine the best achievable performance of MPC.

Simulations run using MPC lead to slightly stronger performance than our two-level algorithm. A comparison between MPC with $\mu = 150$ rounds and OCO is shown in Figure 9 for a several energy resource variables. Note that the two-level algorithm was re-run in the case of OCO and thus different time-varying data (e.g. temperature) were observed because of the uncertainty. The receding horizon was set to $\mu = 150$ steps to ensure that the MPC horizon exceeds the number of tracking rounds, which is $F = 120$, thus guaranteeing that MPC fully leverages its foresight. Because MPC solves an optimization problem at each time step, it meets the scheduled objective more quickly. MPC also makes use of more future information than OCO, and hence has better foresight.

The main advantage of OCO over MPC is scalability. A comparison between the running time of an OCO and MPC-based tracking level is presented in Table V. For example, running the two-level algorithm with OCO takes on average 2.70 minutes compared to 20.43 hours when MPC with $\mu = 150$ is used. In this case, MPC requires a factor of 454 more computation time than OCO. Hence, on average, the MPC update requires 25.5 seconds to compute the energy dispatch at each tracking round as opposed to 0.05 seconds for the OCO algorithm.

The average MPC computation time is almost as long as the duration of the round. In 13.36% of cases the MPC computation took more time than the length of the round. Thus, in these cases the operator would not have an implementable decision. For this reason, OCO is more suitable for real-time energy dispatch of buildings.

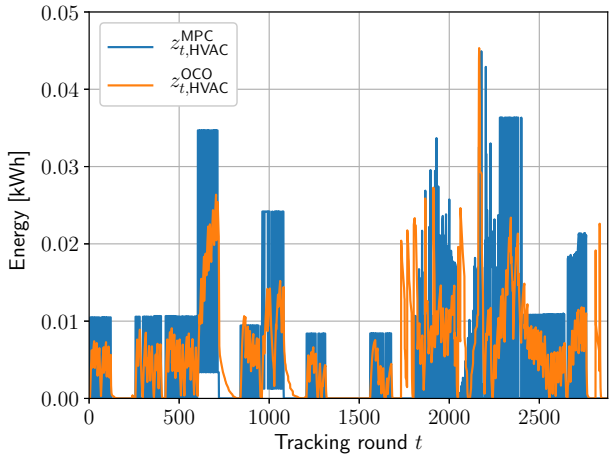

(a) HVAC energy consumption $z^{\text{MPC}}_{t,\text{HVAC}}$ & $z^{\text{OCO}}_{t,\text{HVAC}}$

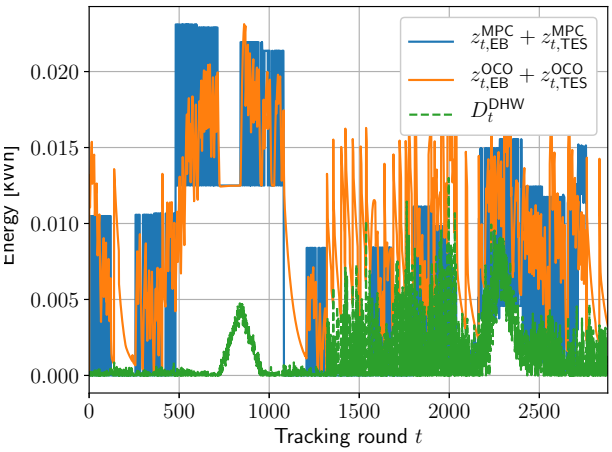

(b) DHW demand $z^{\text{MPC/OCO}}_{t,\text{EB}} + z^{\text{MPC/OCO}}_{t,\text{TES}} \geq D^{\text{DHW}}_t$

Fig. 9. Real-time energy resources usage using MPC as the tracking algorithm

VI. CONCLUSION

We have proposed a two-level algorithm to manage MES under uncertainty. We model a building as an MES with multiple sources of flexibility, energy requirements and access to several electricity markets. We use MILP to schedule hourly energy consumption using mean data about markets and natural phenomena for each hour. We then use OCO to track this consumption objective while facing uncertainty. The performance of our two-level algorithm is assessed in a case study based on a terraced house in Melbourne, Australia. In simulations over a 45-day data set, our approach attained an average net revenue of \$2.03 each day improving over a balance of $-$\$1.62 when no energy management is done. To improve performance, a more detailed building model could be used to make the scheduling level more accurate.

We have shown that a building-based MES can use its flexibility to provide ancillary services. This benefits both the building by increasing its revenue and the grid by contributing to its reliability and grid efficiency. In future work, we will extend our approach to aggregations of multiple buildings providing ancillary services in a network.

REFERENCES

[1] P. Mancarella, "MES (multi-energy systems): An overview of concepts and evaluation models," *Energy*, vol. 65, pp. 1–17, 2014.
[2] E. Fabrizio, V. Corrado, and M. Filippi, "A model to design and optimize multi-energy systems in buildings at the design concept stage," *Renewable Energy*, vol. 35, no. 3, pp. 644–655, 2010.
[3] D. S. Callaway, "Tapping the energy storage potential in electric loads to deliver load following and regulation, with application to wind energy," *Energy Conversion and Management*, vol. 50, no. 5, pp. 1389–1400, 2009.
[4] J. A. Taylor, S. V. Dhople, and D. S. Callaway, "Power systems without fuel," *Renewable and Sustainable Energy Reviews*, vol. 57, pp. 1322–1336, 2016.

[5] L. Zhang, N. Good, and P. Mancarella, "Building-to-grid flexibility: Modelling and assessment metrics for residential demand response from heat pump aggregations," *Applied Energy*, vol. 233, pp. 709–723, 2019.
[6] R. Moreno, R. Moreira, and G. Strbac, "A milp model for optimising multi-service portfolios of distributed energy storage," *Applied Energy*, vol. 137, pp. 554–566, 2015.
[7] L. Paull, H. Li, and L. Chang, "A novel domestic electric water heater model for a multi-objective demand side management program," *Electric Power Systems Research*, vol. 80, no. 12, pp. 1446–1451, 2010.
[8] N. Good, E. Karangelos, A. Navarro-Espinosa, and P. Mancarella, "Optimization under uncertainty of thermal storage-based flexible demand response with quantification of residential users' discomfort," *IEEE Transactions on Smart Grid*, vol. 6, no. 5, pp. 2333–2342, 2015.
[9] D. T. Nguyen and L. B. Le, "Joint optimization of electric vehicle and home energy scheduling considering user comfort preference," *IEEE Transactions on Smart Grid*, vol. 5, no. 1, pp. 188–199, 2014.
[10] H. Wang, N. Good, P. Mancarella, and K. Lintern, "PV-battery community energy systems: Economic, energy independence and network deferral analysis," in *European Energy Market (EEM), 2017 14th International Conference on the*. IEEE, 2017, pp. 1–5.
[11] H. Wang, N. Good, and P. Mancarella, "Modelling and valuing multi-energy flexibility from community energy systems," in *Universities Power Engineering Conference (AUPEC), 2017 Australasian*. IEEE, 2017, pp. 1–6.
[12] ——, "Economic analysis of multi-service provision from PV and battery based community energy systems," in *Innovative Smart Grid Technologies-Asia (ISGT-Asia), 2017 IEEE*. IEEE, 2017, pp. 1–6.
[13] C. E. Garcia, D. M. Prett, and M. Morari, "Model predictive control: theory and practice—a survey," *Automatica*, vol. 25, no. 3, pp. 335–348, 1989.
[14] F. Borrelli, A. Bemporad, and M. Morari, *Predictive control for linear and hybrid systems*. Cambridge University Press, 2017.
[15] R. Z. Freire, G. H. Oliveira, and N. Mendes, "Predictive controllers for thermal comfort optimization and energy savings," *Energy and Buildings*, vol. 40, no. 7, pp. 1353–1365, 2008.
[16] R. Negenborn, M. Houwing, B. De Schutter, and J. Hellendoorn, "Model predictive control for residential energy resources using a mixed-logical dynamic model," in *Networking, Sensing and Control, 2009. ICNSC'09. International Conference on*. IEEE, 2009, pp. 702–707.
[17] F. Oldewurtel, A. Parisio, C. N. Jones, D. Gyalistras, M. Gwerder, V. Stauch, B. Lehmann, and M. Morari, "Use of model predictive control and weather forecasts for energy efficient building climate control," *Energy and Buildings*, vol. 45, pp. 15–27, 2012.
[18] S. Shalev-Shwartz *et al.*, "Online learning and online convex optimization," *Foundations and Trends® in Machine Learning*, vol. 4, no. 2, pp. 107–194, 2012.
[19] E. Hazan *et al.*, "Introduction to online convex optimization," *Foundations and Trends® in Optimization*, vol. 2, no. 3-4, pp. 157–325, 2016.
[20] S.-J. Kim and G. B. Giannakis, "An online convex optimization approach to real-time energy pricing for demand response," *IEEE Transactions on Smart Grid*, vol. 8, no. 6, pp. 2784–2793, 2017.
[21] A. Lesage-Landry and J. Taylor, "Setpoint tracking with partially observed loads," *IEEE Transactions on Power Systems*, vol. 33, no. 5, pp. 5615–5627, 2018.
[22] Australian Energy Market Operator, "Guide to ancillary services in the national electricity market," 2010.
[23] M. J. Neely and H. Yu, "Online convex optimization with time-varying constraints," *arXiv preprint arXiv:1702.04783*, 2017.
[24] T. Chen, Q. Ling, and G. B. Giannakis, "An online convex optimization approach to proactive network resource allocation," *IEEE Transactions on Signal Processing*, vol. 65, no. 24, pp. 6350–6364, 2017.
[25] T. Chen and G. B. Giannakis, "Bandit convex optimization for scalable and dynamic iot management," *IEEE Internet of Things Journal*, 2018.
[26] X. Cao, J. Zhang, and H. V. Poor, "A virtual-queue based algorithm for constrained online convex optimization with applications to data center resource allocation," *IEEE Journal of Selected Topics in Signal Processing*, vol. 12, no. 4, pp. 703–716, 2018.
[27] S. Paternain and A. Ribeiro, "Online learning of feasible strategies in unknown environments," *IEEE Transactions on Automatic Control*, vol. 62, no. 6, pp. 2807–2822, 2017.
[28] M. Mahdavi, R. Jin, and T. Yang, "Trading regret for efficiency: online convex optimization with long term constraints," *Journal of Machine Learning Research*, vol. 13, no. Sep, pp. 2503–2528, 2012.
[29] A. Mokhtari, S. Shahrampour, A. Jadbabaie, and A. Ribeiro, "Online optimization in dynamic environments: Improved regret rates for strongly convex problems," in *Decision and Control (CDC), 2016 IEEE 55th Conference on*. IEEE, 2016, pp. 7195–7201.
[30] J. Nocedal and S. Wright, *Numerical optimization*, 2nd ed. Springer Science & Business Media, 2006.
[31] M. Zinkevich, "Online convex programming and generalized infinitesimal gradient ascent," in *Proceedings of the 20th International Conference on Machine Learning (ICML-03)*, 2003, pp. 928–936.
[32] S. Diamond and S. Boyd, "CVXPY: A Python-embedded modeling language for convex optimization," *Journal of Machine Learning Research*, vol. 17, no. 83, pp. 1–5, 2016.
[33] I. Gurobi Optimization, "Gurobi optimizer reference manual," 2016. [Online]. Available: http://www.gurobi.com
[34] A. Domahidi, E. Chu, and S. Boyd, "ECOS: An SOCP solver for embedded systems," in *European Control Conference (ECC)*, 2013, pp. 3071–3076.
[35] I. Richardson, M. Thomson, D. Infield, and C. Clifford, "Domestic electricity use: A high-resolution energy demand model," *Energy and Buildings*, vol. 42, no. 10, pp. 1878–1887, 2010.
[36] N. Good, L. Zhang, A. Navarro-Espinosa, and P. Mancarella, "High resolution modelling of multi-energy domestic demand profiles," *Applied Energy*, vol. 137, pp. 193–210, 2015.
[37] J. L. Mathieu, M. Kamgarpour, J. Lygeros, G. Andersson, and D. S. Callaway, "Arbitraging intraday wholesale energy market prices with aggregations of thermostatic loads," *IEEE Transactions on Power Systems*, vol. 30, no. 2, pp. 763–772, 2015.
[38] Powerwall, The Tesla Home Battery, "Tesla powerwall." [Online]. Available: https://www.tesla.com/en_AU/powerwall
[39] SunPower, "Sunpower x-series residential solar panels x22-360." [Online]. Available: https://www.sunpower.com.au/sites/international/files/media-library/data-sheets/ds-spr-x22-360-residential-datasheet.pdf
[40] N. H. Reich, B. Mueller, A. Armbruster, W. G. Sark, K. Kiefer, and C. Reise, "Performance ratio revisited: is PR $>$ 90% realistic?" *Progress in Photovoltaics: Research and Applications*, vol. 20, no. 6, pp. 717–726, 2012.
[41] Bureau of Meteorology, "Climate data online." [Online]. Available: http://www.bom.gov.au/climate/data/
[42] Essential Services Commission, "2018–19 feed-in tariffs." [Online]. Available: https://www.esc.vic.gov.au/sites/default/files/documents/key-facts-minimum-feed-in-tariffs-1-july-2018-2018022_v2.pdf
[43] Australian Energy Market Operator, "National electricity market." [Online]. Available: https://www.aemo.com.au/Electricity/National-Electricity-Market-NEM

Antoine Lesage-Landry (M'19) received the B.Eng. degree in Engineering Physics from École Polytechnique de Montréal, QC, Canada, in 2015, and the Ph.D. degree in Electrical Engineering from the University of Toronto, ON, Canada in 2019. He is currently a Postdoctoral Scholar with the Energy & Resources Group at the University of California, Berkeley, CA, USA. His research interests include optimization, online learning and their applications to power system operations.

Han Wang (S'16) received the B.Eng. (Hons.) degree in electrical and electronic engineering from the University of Manchester, Manchester, U.K., and North China Electric Power University, China, in 2015. She is currently pursuing the Ph.D. degree in the Department of Electrical and Electronic Engineering at the University of Melbourne, Melbourne, Australia. Her research interests include modelling of multi-energy systems, optimization of distributed energy resources, and developing associated business cases.

Iman Shames (M'11) is currently a Senior Lecturer at the Department of Electrical and Electronic Engineering, the University of Melbourne. He had been a McKenzie fellow at the same department from 2012 to 2014. Previously, he was an ACCESS Postdoctoral Researcher at the ACCESS Linnaeus Centre, the KTH Royal Institute of Technology, Stockholm, Sweden. He received his B.Sc. degree in Electrical Engineering from Shiraz University in 2006, and the Ph.D. degree in engineering and computer science from the Australian National University, Canberra, Australia in 2011. His current research interests include, but are not limited to, optimisation theory and its application in control and estimation, mathematical systems theory, and security and privacy in cyber-physical systems.

Pierluigi Mancarella (M'08–SM'14) received the MSc and PhD degrees in electrical energy systems from the Politecnico di Torino, Torino, Italy, in 2002 and 2006, respectively. He is currently Chair Professor of Electrical Power Systems at The University of Melbourne, Australia, and Professor of Smart Energy Systems at The University of Manchester, UK. His research interests include multi-energy systems, power system integration of low-carbon technologies, network planning under uncertainty, and risk and resilience of smart grids. Pierluigi is an Editor of the IEEE Transactions on Power Systems and of the IEEE Transactions on Smart Grid, an Associate Editor of the IEEE Systems Journal, and an IEEE Power and Energy Society Distinguished Lecturer.

Josh Taylor (M'11) is an associate professor in the Department of Electrical and Computer Engineering at the University of Toronto. He received the B.S. from Carnegie Mellon University in 2006 and the Ph.D. from the Massachusetts Institute of Technology in 2011, all in Mechanical Engineering. From 2011 to 2012, he was a postdoctoral researcher at the University of California, Berkeley. His research focuses on control and optimization of power systems.